Monsanto

November 1997

Development of an Integrated *in-situ* Remediation Technology

Topical Report for Task #3.2 Entitled, "Modeling and Iron Dechlorination Studies" (September 26, 1994 - August 31, 1997)

Andrew P. Shapiro, Timothy M. Sivavec, and Jan M. Principe

General Electric Research and Development, Box 8

Schenectady, NY 12301

DOE Contract Number: DE-AC05-96OR22459

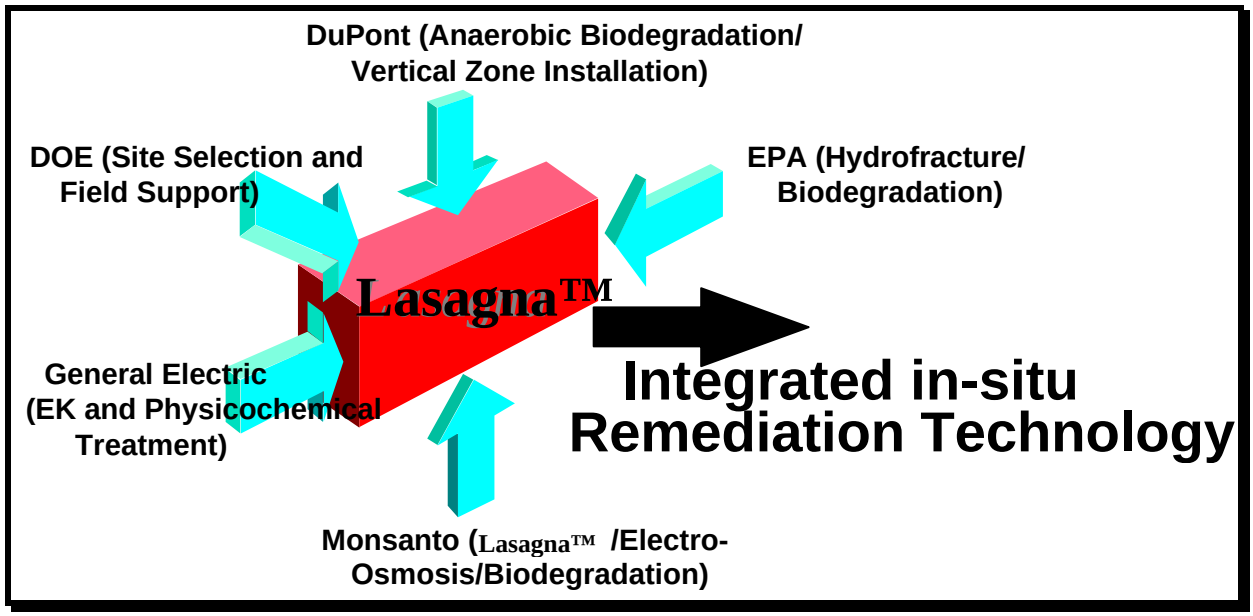

Submitted to:
U. S. Department of Energy
Morgantown Energy Technology Center
Morgantown, West Virginia

Submitted by:
Monsanto Company
800 N. Lindbergh Boulevard
St. Louis, Missouri 63167

TM- A Trademark of Monsanto Company

Development of an Integrated *in-situ* Remediation Technology

DOE Contract Number: DE-AC05-96OR22459

Topical Report for Task # 3.2 - "Modeling and Iron Dechlorination Studies" (January 18, 1996 - August 31, 1997)

Submitted by:

Andrew P. Shapiro, Timothy M. Sivavec, and Jan M. Principe
General Electric Research and Development
P.O. Box 8, Schenectady, NY

Abstract

Contamination in low-permeability soils poses a significant technical challenge to in-situ remediation efforts. Poor accessibility to the contaminants and difficulty in delivery of treatment reagents have rendered existing in-situ treatments such as bioremediation, vapor extraction, and pump and treat rather ineffective when applied to low-permeability soils present at many contaminated sites. The technology is an integrated in-situ treatment in which established geotechnical methods are used to install degradation zones directly in the contaminated soil, and electro-osmosis is utilized to move the contaminants back and forth through those zones until the treatment is completed. The present Topical Report for Task #3.2 summarizes the modeling and dechlorination research conducted by General Electric Research and Development.

B. Acronyms and Abbreviations

DCE	Dichloroethylene
DNAPL	Dense Non-Aqueous Phase Liquid
DOE	Department of Energy
DuPont	E. I. du Pont de Nemours & Co., Inc.
EPA	Environmental Protection Agency
GC	gas chromatography
GE	General Electric Company
LMES	Lockheed Martin Energy Systems
ROD	Record of Decision
RREL	Risk Reduction Engineering Laboratory
SWMU	Solid Waste Management Unit
TCE	trichloroethylene
VC	vinyl chloride

C. Units

C, ˚C	Celsius, degrees Celsius
cm	centimeters
d, D	days
deg	degrees
F, ˚F	Fahrenheit, degrees Fahrenheit
f, ft	feet
g	grams
gal, GAL	gallons
h, hr	hours
in	inches
k, K	thousand
kg	kilograms
l, L	liters
lb, lbs	pound(s)
m	meter
mg	milligrams
min	minutes
ml, mL	milliliters
mm	millimeters
ppb	parts per billion
ppm, ppmw	parts per million (by weight)
psi	pounds per square inch
µg	micrograms
µl, µL	microliters
"	inches
'	feet
#	pounds

D. Table of Contents

List of Tables

List of Figures

List of Figures (cont'd)

E. Background

Statement of the Problem

Contamination in low permeability soils poses a significant technical challenge to *in-situ* remediation efforts. Poor accessibility to the contaminants and difficulty in delivery of treatment reagents have rendered existing *in-situ* treatments such as bioremediation, vapor extraction, and pump and treat, rather ineffective when applied to low-permeability soils present at many contaminated sites.

The Solution

The proposed technology combines electro-osmosis with treatment zones that are installed directly in the contaminated soils to form an integrated *in-situ* remedial process. Electro-osmosis is an old civil engineering technique and is well known for its effectiveness, utilizing very low power consumption, in moving water uniformly through low-permeability soils.

Conceptually, the integrated technology could treat organic and inorganic contamination, as well as mixed wastes. Once developed, the technology will have tremendous benefits over existing ones in many aspects including environmental impacts, cost effectiveness, waste generation, treatment flexibility, and breadth of applications.

Consortium Description

A Consortium has been formed consisting of Monsanto, E. I. du Pont de Nemours & Co., Inc. (DuPont), and General Electric (GE), with participation from the Environmental Protection Agency (EPA) Office of Research and Development, and the Department of Energy (DOE) Environmental Management Office of Science and Technology. The five members of this group are leaders in their represented technologies and hold significant patents and intellectual property which, in concert, may form an integrated solution for soil treatment. The figure on the cover page shows a schematic diagram of the various technologies which the government/industry consortium has integrated for the development of an *in-situ* remediation technology.

Project History

To date, this project has been conducted in two parts: Phase I and Phase IIa. A Management Plan was originally prepared for Phase I of this project by Monsanto and submitted on November 30, 1994. That plan summarized the work plan which was developed in conjunction with DuPont, GE, EPA's Risk Reduction Engineering Laboratory (RREL), Lockheed Martin Energy Systems (LMES), and the Department of Energy. The DOE Gaseous Diffusion Plant in Paducah, Kentucky, was chosen as the site for the initial field tests. The specific contamination site selected at the Plant was Solid Waste Management Unit (SWMU) 91. For Phase I, the plot selected to demonstrate the process measured 10 feet by 15 feet by 15 feet deep.

CDM Federal Programs Corporation was chosen to provide the on-site support of the field tests which were installed at the DOE site in November 1994. This experiment tested

the combination of electro-osmosis and *in-situ* sorption in the treatment zones. Technology development was carried out under the present contract in Phases I and IIa by Monsanto, DuPont, and GE. These studies evaluated various degradation processes and their integration into the overall treatment scheme at bench and pilot scales.

Phase IIa was approved on January 18, 1996. For this phase, a significantly larger plot was selected, measuring 21 feet by 30 feet by 45 feet deep, and significant design changes were also implemented in the materials used to construct the electrodes and treatment zones. While Phase I was conducted to demonstrate the movement of TCE from the soil into the treatment zones, Phase IIa was conducted to demonstrate the full scale remediation of the SWMU 91 site. This latter phase included the use of zero valent iron metal which degrades TCE to light hydrocarbons and chloride ions. In August of 1997, DOE advised that, based upon the performance of the *Lasagna*™ process during Phases I and IIa, *Lasagna*™ would be the preferred remedy given in the proposed Record of Decision (ROD). If signed, this ROD will be the first example of the use of *Lasagna*™ for the full scale remediation of a TCE-contaminated clay site. ROD approval is expected in calendar-year 1998.

Technical Deliverables

Table E-1 lists the four topical reports which have been written to describe the results obtained from the Phase IIa research. This table also shows which organization is primarily responsible for the tasks and for preparing the topical reports. The present topical report summarizes Task #3.2.

Table E-1. List of Topical Reports and Responsible Company

Topical Report	Company
Task #3.1 - Emplacement Technology	DuPont
Tasks #3.2 - Modeling and Iron Dechlorination Studies	GE
Task #3.3 - *Lasagna*™ and Iron Dechlorination	Monsanto
Task #7.2 - Field Scale Test	Monsanto/DuPont/GE

F. Treatment Zone and Electrode Characteristics

The work reported in Topical Report for Task 9 in Phase I demonstrated the ability of iron zones to dechlorinate TCE in an electro-osmotic flow field. The issues of flow cessation due to hydrogen evolution within the treatment zone and the presence of daughter products from incomplete dechlorination were identified as areas requiring more development for commercializing the *Lasagna*™ process. In the interim between the end of Phase I and the beginning of Phase IIa, researchers at GE and Monsanto identified that clay and iron mixtures were effective in solving the problem of flow cessation due to gas evolution. In addition, studies on the reactivity of iron provided design criteria to ensure adequate dechlorination of all daughter products. Investigated treatment zones included coarse iron filings (8x50 mesh), fine iron filings (<40 mesh), mixtures of sand and iron, and mixtures of kaolin clay and iron. All systems that did not contain clay as a filler material exhibited gas accumulation in the treatment zone. The experiments begun under this task, which do in fact verify the performance of the iron/clay mixtures, were conducted for long periods of time and are therefore reported below under Task 3.2.1.3 (Life of Iron Treatment Zones).

During the design of Phase IIa, several issues were identified regarding the design of electrode zones. Therefore the scope of this task was extended to included studies on some key issues involving the characteristics of the electrode zones. These studies are reported here.

Conductivity tests of electrode mixture

One of the proposed methods to emplace electrodes in soil involves pumping a slurry of electrode material down the mandrel as it is withdrawn from the hole. To form a pumpable slurry of coarse grained particles, such as those proposed for the *Lasagna*™ electrodes, chemicals are often added to the water to make a more viscous suspension. The increased viscosity slows drainage of the fluid from the suspension and thereby decreases the likelihood of bridging of the particles and clogging of the piping. In addition, the increased viscosity is expected to enable a more uniform blend of dissimilar particles to be delivered to the electrode zone. One of the viscosifying agents being considered for the *Lasagna*™ electrodes is guar gum. Guar is a plant-derived polymer that is easily broken down by microorganisms. Small amounts of guar dissolved in water greatly increase the fluid viscosity. Enzyme breakers can be added to accelerate the degradation of the guar.

Experiments were conducted to determine the effect of guar gum and breaker on the electrical conductivity of the saturated granular electrode material. The electrode is composed of coke and iron particles saturated with water. The coke material is a conductive form of carbon used in cathodic protection applications. The coke is expected to be electrochemically inert and should maintain the high hydraulic permeability in the electrode region required for gas evolution and water circulation. The iron acts as a pH buffer at the anode. This buffering function may be accomplished by direct electrochemical oxidation of the iron metal, or neutralization by the iron of hydronium ions generated electrochemically at the coke surface. Both mechanisms yield ferrous ions in solution.

Experimental method

A mixture of 48.7 wt% Peerless iron (-20 mesh Type IS) and 51.3 wt% Loresco SWS coke was prepared by combining dry ingredients in a jar and rolling the jar on a mill for several hours. A guar gum solution was prepared by mixing guar obtained from Halliburton, Inc. (WG-19) with

tap water at a ratio of 4.8 g guar per liter of solution (40 lb/1,000 gal). Two 50-ml samples of guar solution were removed. To one sample, 0.0026 g of an enzyme breaker (GBW-30) obtained from Halliburton was added. Three saturated electrode mixtures were prepared as indicated in Table F-1.

Table F-1. Electrode Sample Compositions

Coke Iron Mass (g)	Liquid Added (ml)
97.7	50 ml guar solution, no breaker
97.5	50 ml guar solution with breaker
97.7	50 ml tap water (dried out during test)
97.7	50 ml tap water

Eighty grams of each mixture were loaded into plastic cylindrical vials. The internal diameter of the vials was 3.3 cm, and the height of the packed mixture ranged from 3.2 to 4.0 cm. The bottom of the vial was lined with a copper foil, which served as one electrode for the conductivity measurements. An insulated wire lead soldered to the foil ran up the inner wall of the vial and extended out of the vial. Another copper foil electrode with soldered wire lead was placed in contact with the top of the electrode matrix. A Hewlett-Packard ESR meter was used to measure resistance at 1,000 Hz. Resistance was measured with and without compression from a vertical load equivalent to 68 KPa (10 psi). The conductivity of the electrode material was determined from the following relation:

$$s = \frac{L}{AR}$$

where σ is the electrical conductivity in Ω^{-1} m^{-1}, L the height of the packed electrode (m), and A the cross sectional area (m^2).

Results

The results of the resistance measurements are shown in Figure F-1. It is clear from these measurements that the guar gum causes a significant reduction in conductivity of the packed bed of coke and iron. The breaker apparently does not have any effect in improving the conductivity with time. One of the test runs without guar (case "a") had a relatively high conductance initially; however, the conductivity dropped substantially during the test. The reason for the decrease in conductivity in this case was loss of water through a crack in the container, which resulted in oxidation of the iron exposed to air, which in turn, resulted in decreased conductivity. When this experiment was repeated (case "b") with a non-leaking apparatus, the conductivity of the coke/iron mixture remained high compared to the guar gum samples.

The important parameter in determining acceptable conductivity for the electrode mixture is the ratio of electrode to soil conductivity times the product of the electrode thickness and electrode spacing (σ_e/σ_s X tL). The square root of this parameter is the length scale over which the voltage applied to the surface of the electrode exponentially decays with depth. Thus, for 5 cm thick electrodes spaced 6.4 m apart with electrode conductivity σ_e=40 S/m (similar to the no guar case) and soil conductivity σ_s=0.024 S/m, decay length is 23 m. For this case the voltage at the surface of the electrode will be very close to that at a depth of 15 m. However, if the electrode conductivity were σ_e=5 S/m (similar to the guar case), the decay length would be 8.1 m. This means that the electric field at 15 m depth would be approximately 16% of that applied at the

surface. Therefore the use guar gum as a viscosifying agent for the electrode slurry is not recommended.

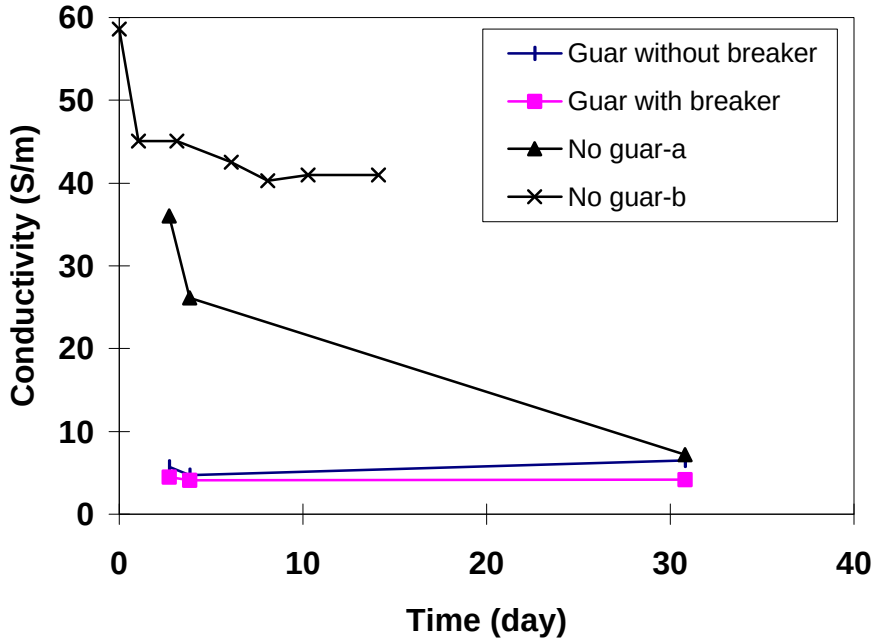

Figure F-1. Conductivity of electrode mixture vs. time.

Clay-Permeating Electrode Studies

The design of the electrode zones in Phase IIa calls for a mixture of granular iron and conductive coke to be poured into a 45-ft deep, 2-inch thick slot made in the soil by pushing a mandrel to depth with a vibrating hammer. The conductivity of the electrodes is important for maintaining a uniform electric field in the soil and for ensuring energy-efficient operation. One scenario identified as a potential problem was the possibility of soil surrounding the electrode mixture permeating the electrode because of compressive stresses that might exist in the soil if it is overconsolidated, or that might be generated by the mandrel insertion process. If the surrounding soil permeated the electrode material, the electrode's conductivity would be compromised. Several experiments were conducted in the laboratory to determine the likelihood of this failure mechanism.

Experimental methods

The first experiment examined the behavior of a cylindrical core of electrode material surrounded by an annulus of consolidated kaolin clay in a triaxial compression cell. A triaxial compression cell permits a cylindrical sample to be subjected to an overall hydrostatic pressure while a one-dimensional pressure gradient is applied in the axial direction of the cylinder. The hydrostatic pressure can be adjusted independently of the pressure gradient to represent the total soil pressure at a desired depth. The hydrostatic pressure is transmitted to the sample through a silicone rubber sleeve that conforms to the cylinder's surface while preventing permeation in the radial direction. The one-dimensional pressure gradient can represent a typical groundwater gradient or can be used to calculate the soil permeability. The pressure gradient is applied to the face plates that compress the right faces of the cylinder and are sealed to the silicone sleeve by o-

rings. The triaxial apparatus used in these experiments was a Brainard /Kilman S-500 system with a S-510 test cell.

The sample used in the first test was constructed as follows: A 40% water/60% EPK kaolin clay (w/w) mixture was formed into a 2-inch diameter by 3-inch long cylinder and placed in the triaxial cell. A hydrostatic pressure of 40 psig was applied for 24 h to consolidate and dewater the clay. Forty psi represents the expected hydrostatic force on soil at a depth of approximately 45 feet. The pressure at both face plates was maintained at 10 psig so that excess water could be drained from the sample through both faces. After consolidation, the sample was removed from the test cell and the face plates detached from the silicone sleeve. With the sleeve still on the sample, a 0.9-inch core was removed from the center of the sample with a cork boring tool. The empty core was backfilled with the electrode mixture (50% Peerless iron/ 50% Loresco SWS coke (w/w)). The sample faces were trimmed squarely so the final cylinder length was 2.4 inches. The face plates and filter paper were reattached to the sample and sleeve according the manufacturer's instructions. The sample was put back in the triaxial test cell, and a 40-psi hydrostatic pressure was again applied. Five psi was maintained at the faces of the cylinder. Because of the extremely large ratio of core-to-clay permeability, the pressure within the core was also nearly 5 psi. After 16 h of consolidation, the permeability of the sample was measured. Unfortunately, the hydraulic resistance of the frits used in the face plates was much higher than that of the electrode material in the core, so accurate measurements of the core permeability could not be made. After 6 days of 40 psi hydrostatic pressure and 5 psi in the core, the sample was removed from the test cell and then sectioned and photographed.

The second experiment investigating the permeation of clay into the electrode mixture used clay soil from the Paducah test site. In this experiment a cylinder of clay 3.9 cm in diameter was sliced into two pieces 3.7 and 3.5 cm thick. A 1.7-cm thick disk, 3.9 cm in diameter, of the iron/coke mixture was placed between the clay sections. The three sections were held together by a latex sleeve. The experimental setup is shown in Figure F-2. The sample was compressed in a Carver press for 20 minutes at a load ranging from 105 to 158 psi. This load was much higher than the soil would be subjected to in the in the field. The sample was sliced into sections after compression and visually inspected for evidence of clay permeating the iron/coke mixture.

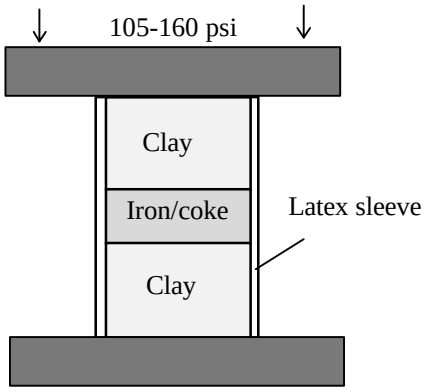

Figure F-2. Apparatus for compression test on iron/coke mixture.

Results

The results of both tests showed no penetration of clay into the mixture. In the triaxial compression test, the core remained free of clay particles. In the one-dimensional compression test, the clay sections bulged out under the load, but no clay penetration of the iron zone was observed. These results are encouraging for the use of iron/coke mixtures for electrodes in the *Lasagna*™ process. It must be noted that these test do not address the issue of migration of clay particles by electrophoresis or precipitation of oxides and hydroxides, both of which may lead to reduced conductivity of the electrodes with time. The field test conducted in Phase IIa will address these issues.

G. Gas Evolution Study

Preliminary studies on using iron particles for treatment zones in electrokinetic remediation identified gas evolution as a potential problem. Hydrogen gas evolves from the corrosion of iron in water according to the reaction

$$Fe^0 + 2H_20 \rightarrow Fe^{2+} + 2OH^- + H_2(g)$$

The rate of hydrogen evolution depends on several factors, including pH, temperature, and water chemistry. In this application, the presence of an applied electric field may also influnce the corrosion rate. Iron corrosion has been studied in application to permeable barriers in conjunction with groundwater decontamination (Reardon 1995), and the results of that study are compared to the measurements made in this work.

Experimental method

The apparatus used in these tests, shown in Figure G-1, was constructed from a 50-ml serum vial which can be sealed by a septum and a crimped aluminum collar. A glass U-tube (0.49 cm ID) was connected to the neck of the serum vial. This U-tube was partially filled with water before the vial was filled and sealed, so that a manometer was formed in the tube. Iron filings (Peerless IS <20 mesh) were mixed with kaolin clay (EPK) saturated with nitrogen-purged tap water. The weight ratio of the iron/clay/water mixture was 20:46:34. Ten grams of the mixture were placed in a modified serum vial. Approximately 40 ml of nitrogen-purged tap water was added to the vial to bring the water level up to the point where the U-tube was connected.

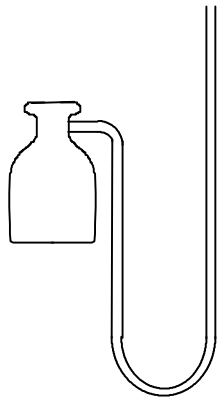

Figure G-1. Apparatus used in gas evolution studies.

After the vial was filled with water, a Teflon-lined septum was crimped tightly in place. By measuring the height difference of the water columns on the two sides of the U-tube, the change in internal pressure could be determined. The change in pressure is directly related to the mass of gas in the vial. The vial was left at room temperature for up to 160 days.

Results and Discussion

The vial pressure versus time is plotted in Figure G-2. The transient behavior is characterized by an initial decrease in pressure followed by a steady pressure increase.

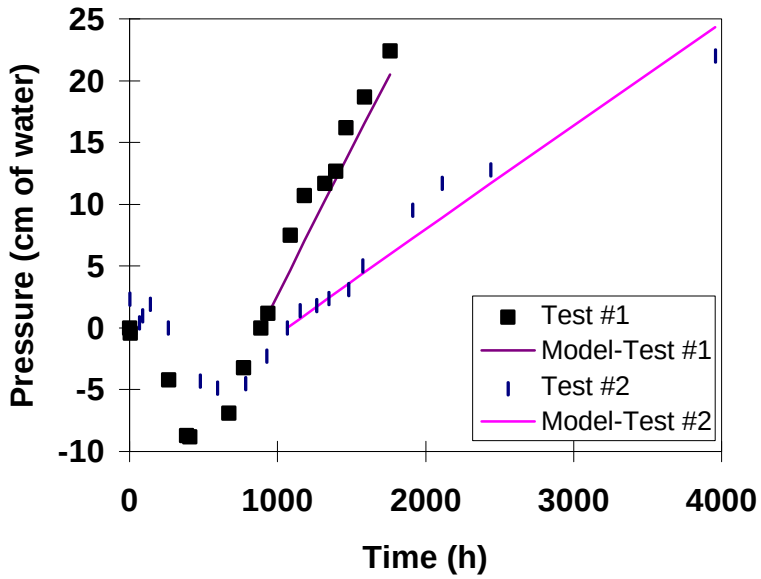

Figure G-2. Pressure change vs. time in enclosed vial of iron, clay, and water. Model curve fits yield $5.2\ 10^{-5}$ and $1.9\ 10^{-5}$ μmol/s for tests #1 and #2 respectively.

The initial decrease can be attributed to consumption of the oxygen initially present in the headspace. In the presence of oxygen, a probable corrosion reaction for iron is

$$4Fe^0 + 3O_2 \rightarrow 2Fe_2O_3 \qquad \textbf{Eq. 1}$$

This reaction causes the iron in the clay mixture to act as a sink for any oxygen in the vial. The steady increase in pressure later in the experiment is attributable to the generation of hydrogen according to the reaction

$$Fe^0 + 2H_2O \rightarrow Fe^{+2} + 2OH^- + H_2(g) \qquad \textbf{Eq. 2}$$

To determine the rate of hydrogen evolution in this experiment, the initial period during which the pressure decreased was neglected. To relate the rate of gas evolution to the manometer reading, we assume ideal gas behavior and account for the changing gas volume as the manometer fills. The ideal gas relation is

$$P = nRT/V \qquad \textbf{Eq. 3}$$

where P is the absolute pressure, n the number of moles of gas, R the ideal gas constant, T the absolute temperature and V the gas volume. Assuming a constant rate of gas generation, the number of moles of gas, n, is given by

$$n = n_0 + rt \qquad \textbf{Eq. 4}$$

where t is time, n_0 is the number of moles at t=0, and r the rate of gas evolution or the corrosion rate.

As the gas generated pushes the manometer fluid in the U-tube, the gas volume, *V*, changes according to

$$V = V_0 + A(h-h_0) \qquad \textbf{Eq. 5}$$

where V_0 is the initial gas volume, A the cross-sectional area of the U-tube, h is the height difference between water columns in the U-tube, and h_0 is the height difference at t=0. The initial pressure in the vial is

$$P_0 = n_0 RT/V_0 \qquad \textbf{Eq. 6}$$

The pressure in the vial is related to the manometer reading by

$$P = P_0 + \rho g \Delta h \qquad \textbf{Eq. 7}$$

where ρ is the density of water, g the acceleration of gravity, and Δh the change in height difference, $h-h_0$, between manometer columns. Combining Eq. 3 and Eq. 7, grouping like ordered terms in Δh yields

$$\Delta h^2 + \frac{\rho g V_0 + P_0 A}{\rho g A}\Delta h - \rho t \frac{RT}{\rho g A} \qquad \textbf{Eq. 8}$$

This quadratic Eq. can be solved for Δh to give

$$\Delta h = 0.5\left(-b + \sqrt{b^2 + \frac{4\rho t RT}{\rho g A}}\right) \qquad \textbf{Eq. 9}$$

where $\beta = \frac{\rho g V_0 + P_0 A}{\rho g A}$.

In these experiements, the value of β is two orders of magnitude higher than typical values of Δh. In these cases Eq. 9 can be simplified to yield the linear relation

$$\Delta h = \rho t \frac{RT}{\rho g V_0 + P_0 A} \qquad \textbf{Eq. 10}$$

The data for the two experiments are shown in Figure G-2. The initial decrease in pressure is attributed to the consumption of oxygen dissolved in the water by the oxidizing iron. Equation 9 was fitted with the data for times after the effects of oxygen consumption were observed. The adjustable parameters are *r*, the corrsion rate, and V_0, the initial gas volume. The values of the relavent parameters are listed in Table G-1.

Table G-1. Parameters used in model curve

Parameter	Symbol (units)	Value
Initial pressure	P_0 (N/m^2)	1 X 10^5
Initial gas volume	V_0 (m^3)	4.9 X 10^{-6}
Ideal gas constant	R (J/mol/K)	8.314
Absolute temperature	T (K)	293
Water density	ρ (kg/m^3)	1,000
Accleration of gravity	g (m^2/s)	9.8
Cross-sectional area of U-tube	A (m^2)	1.88 X 10^{-5}

The corrosion rate determined by the curve fit is 4.5 10^{-3} mmol/d and 1.6 X 10^{-3} mmol/d for tests 1 and 2 respectively. Normalizing by the mass of iron in the experiment gives a specific corrosion rate of 2.2 and 0.8 mmol/kg/day. These values are slightly higher than the corrosion rates published by Reardon (ES&T '95, **29,** 2936-2945), which ranged from 0.1 to 0.7 mmol/kg/day. The higher rates measured in these tests compared to those of Reardon may be attributable to the fact that, in these tests, the iron was mixed with clay, which had a buffering effect on the pH. At the end of both tests the solution pH was 5.5. In Reardon's tests the pH was consistently over 7.7 and usually over 9.5. According to Eq. 2, a lower pH should cause the corrosion of iron to be faster because the OH^- concentration on the product side is reduced.

One of the reasons for concern over the generation of hyrodgen is the possibilty of creating an explosive environment. The results of these tests indicate that for a treatment zone 5 cm thick by 15 m deep with 7% (vol/vol) iron, the steady-state flux of hydrogen permeating to the surface of the treatment zone would be approximately 16 moles of H_2 per square meter per day, assuming a corrosion rate of 2.2 mmol/kg/day. Assuming a mass transfer coefficient of 0.5 $mol/m^2/s$, typical of natural convection, the expected hydrogen concentration at the surface of the treatment zone would be 370 ppm. This hydrogen concentration would be the maximum expected at the soil surface where oxygen is available for combustion. The concentration is well below the lower explosion limit for hydrogen (18%), and therefore dangers associated with hydrogen combustion are insignificant.

H. Life of Iron Treatment Zones

In Phase I GE/CRD demonstrated the feasibility of using iron metal for treatment zones in the *Lasagna*™ process (see Topical Report, Task 9) to dechlorinate TCE. In electrokinetic cell experiments, TCE was shown to dechlorinate as electro-osmosis forced the water carrying it through a 1-inch zone of iron particles sandwiched between two saturated clay layers. These experiments indicated that, with a residence time in the iron zone of approximately 7 h, 96% of the TCE was dechlorinated. Batch and column experiments without electrokinetic effects were conducted to determine the kinetics of TCE dechlorination in the presence of iron (see Topical Report, Task 9). These batch and column experiments demonstrated first order behavior for the sequence of reactions that take TCE to chloride ions and ethene and ethane gas. In addition, the apparent half-life for TCE in the electrokinetic cell (90 min) and the batch experiments (30 min) were comparable when normalized for the surface area of the iron.

The issues identified in Phase I requiring additional investigation were (1) the ceasing of flow attributed to hydrogen gas generation from the corrosion of iron, (2) the persistence of daughter products, such as cis-DCE, which have a longer half life than TCE (3) verification of the dechlorination rates, and (4) long-term performance of the iron zones. Preliminary tests conducted at GE/CRD and Monsanto indicated that a zone composed of a mixture of iron and clay would avoid flow stoppage by preventing the zone from drying out because of gas generation. The experiments reported in this section address the long-term performance of the iron/clay treatment zones and the fate of the daughter products.

Experimental methods

The test cells were cylindrical glass columns (20 cm x 5 cm dia.) shown schematically in Figure H-1. A feed solution containing TCE at a nominal concentration of 100 ppm was fed into a chamber at the anode side of the cell. Electro-osmosis drove some of the feed solution toward the cathode. Enough feed solution was supplied to permit some solution to overflow the chamber so that nearly constant conditions could be maintained in the chamber. This feed chamber was separated from the anode chamber by a Nafion® cation exchange membrane. Two reasons for using the membrane were to prevent TCE from being stripped by the oxygen bubbles generated at the anode, and to permit the chloride ions generated in the iron zone, as a result of dechlorination, to be collected with the feed overflow. The column end caps used to form the catholyte, anolyte, and purging chambers were made from Teflon and sealed using Teflon-covered silicone o-rings.

The materials used to form the test samples and the electrodes in these experiments are listed in Table H-1. A test sample was assembled by placing approximately 175 g of a saturated kaolin clay mixture (40% (w/w) water) in one end of the glass cylinder. A porous carborundum disk lined with glass fiber filter paper formed a porous support that could slide in the cylinder but fit snugly enough to confine the clay sample. Air bubbles were removed from the clay by tapping the base of the cylinder, porous support side down, on a table. After smoothing the open surface of the clay, approximately 100 g of treatment zone mixture was placed on the clay section. Again, tapping the cylinder removed air bubbles and the top surface of the treatment zone was flattened. The final section of approximately 175 g of clay was placed on top of the treatment zone mixture, and tapped to removed air bubbles. Another filter-paper-lined porous disk was pushed into the open end of the cylinder and pressed against the clay sample. The Teflon end-pieces forming the electrolyte chambers, and holding the cation exchange membrane, were placed on the ends of the

cylinder and bolted together with three 0.95-cm diameter threaded rods, which extended the length of the test cell. Finally a set of three 0.32-cm diameter rods, which penetrated the cathode end-piece though Teflon compression fittings, were pushed by a backing plate, restrained by bolted threaded rods, to apply pressure to the porous disk. The nuts constraining the backing plate were finger-tightened periodically for approximately 1 week to dewater and consolidate the test sample. By measuring the change in volume of the test sample during the consolidation period, and attributing that volume to displaced water, the pore volume of the sample could be calculated.

The TCE concentration of the effluent, feed, and overflow was monitored periodically throughout the experiments. TCE concentrations were determined by hexane extraction followed by gas chromatography/electron capture detection. Periodically, analysis was conducted using purge and trap extraction on 1 and 5 ml aqueous samples followed by gas chromatography/flame ionization detection or mass spectrophotometry. These methods enabled the detection of daughter products of dechlorination, such as cis-DCE, vinyl chloride, ethane, and ethene. Chloride concentration of the overflow was monitored to verify the dechlorination process. The applied current and voltage distribution was also measured through the experiment. At the end of the tests, clay samples were chilled and then divided and extracted to determine the final TCE distribution.

Results

Experiment 1. Coarse iron

Experiment 1 was the first experiment that investigated the long-term performance of iron treatment zones. The iron used in this experiment was Peerless 8 x 50 mesh size iron. The particle size range was from approximately 0.01 to 0.1 inch diameter. The flow through the cell is shown in Figure H-2 where the effluent volume is expressed in terms of pore volumes through the entire cell. The pore volume for this experiment was 101 ml. For the first 260 h, 10 V was applied across the 13-cm clay sample. The initial flow rate was quite high; the electro-osmotic permeability calculated from the initial flow rate was 2.3×10^{-5} cm^2/Vs. The applied voltage was decreased to 5 V after 260 h, and the flow was observed to gradually decrease and actually cease after approximately 1,000 h. The reason for flow cessation was determined to be accumulation of gas in the iron/clay treatment zone. In previous experiments (Phase I report) it was determined that the gas was hydrogen, which formed as a result of iron metal corrosion by water. Once the gas was vented from the cell, the electro-osmotic flow resumed. At 1,600 h the voltage was increased to 10 V, and the flow rate increased and remained very constant for the next 6,000 h. The long-term electro-osmotic permeability was 7.6×10^{-6} cm^2/Vs.

Table H-1. Experimental conditions for long term tests.

Experiment	Clay	Treatment Zone	Electrodes
1. Peerless-coarse	60% Kentucky-Tennessee kaolin 40% water	20 %Peerless 8x50 mesh iron 48% K-T kaolin 32% water 1 inch thick	iron anode stainless steel cathode cation exchange membrane at anode
2. VWR-fine	60% EPK kaolin 40% water	20 %VWR fine iron (<40 mesh) 48% EPK kaolin 32% water 1 inch thick	iron anode stainless steel cathode cation exchange membrane at anode
3. Peerless-fine	60% EPK kaolin 40% water	29% Peerless fine iron 35%Thiele kaolin 35% water 2 inches thick	50% Peerless fine iron 50% Loresco SWS coke saturated with 0.001M Na_2SO_4 cation exchange membrane at anode
4. No iron metal I	Paducah clay	none	iron anode stainless steel cathode cation exchange membrane at anode
5. No iron metal II	Paducah clay	none	iron anode stainless steel cathode cation exchange membrane at anode and cathode

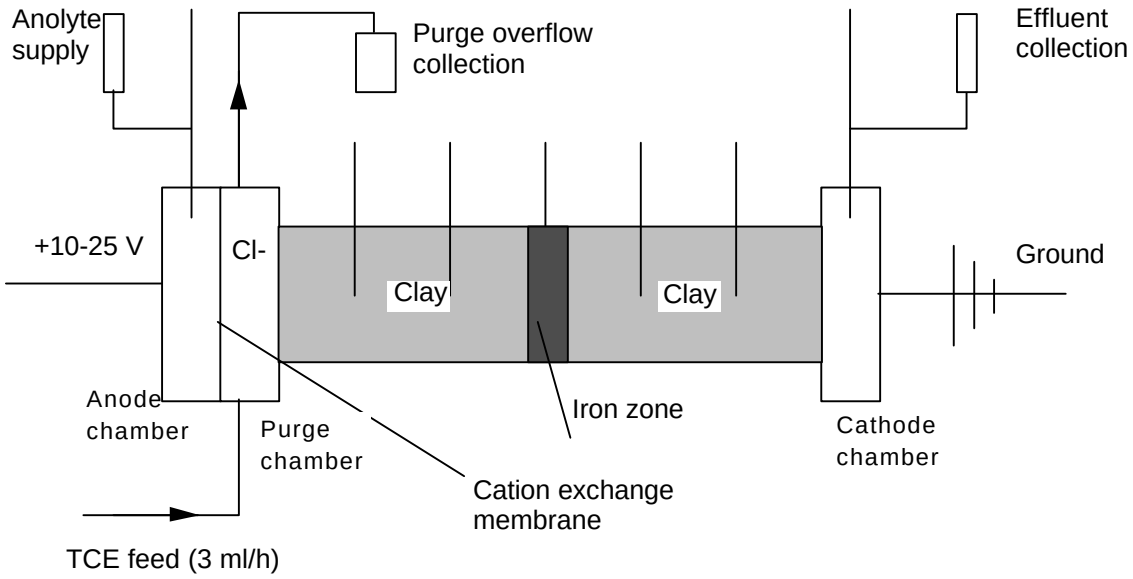

Figure H-1. Schematic of apparatus used in iron zone electrokinetic experiments.

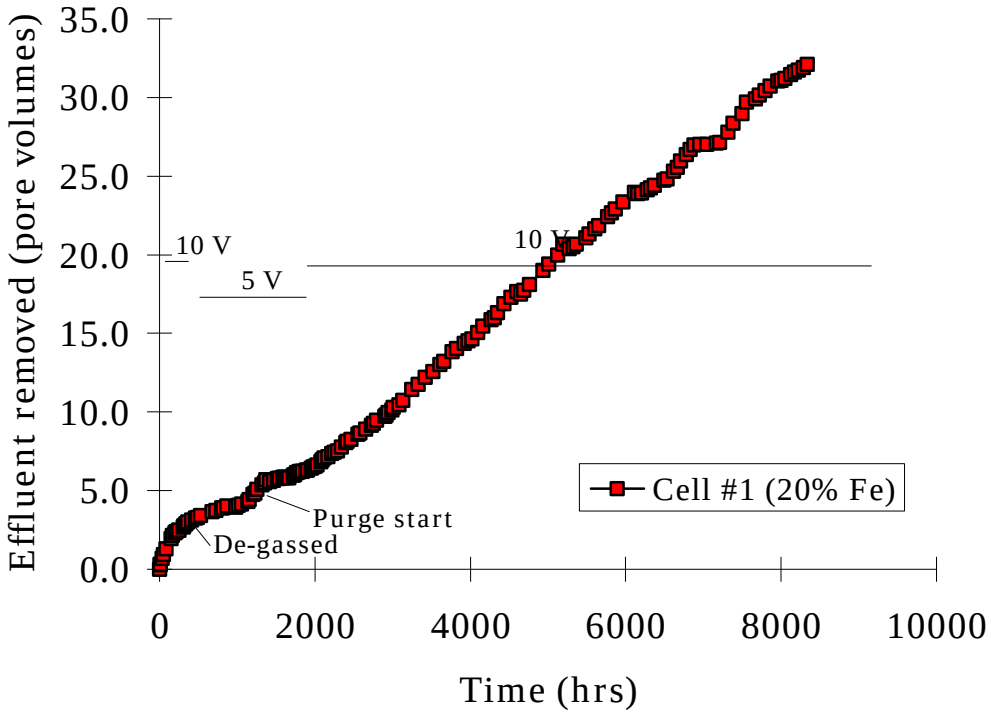

Figure H-2. Flow rate in Experiment 1.

The effectiveness of the treatment zone for dechlorinating TCE is shown in Figure H-3 where the mass of chloride removed in the purge solution is compared to the amount of TCE input into the cell. From the slopes of theses curves, one can estimate the rate of chloride production and TCE introduction. Over most of the experiment, the ratio of these rates is nearly stochiometric at 3 moles Cl^- per mole TCE. The expected accuracy of these measurements is approximately 10%, based on accuracy TCE and chloride analysis and volume measurements. Care was taken not to introduce sources of chloride during the operation of the experiment. While there may have been

some chloride initially adsorbed on the clay, this would be removed in the time it takes to purge a few pore volumes of effluent. The chloride travels the opposite direction as the water; however, its speed should be nearly 5 to 10 times higher than electro-osmosis. A plot of chloride removed versus TCE input is shown in Figure H-4. The best-fit linear regression has a slope of 2.96. Again, the expected uncertainty in these measurements is approximately 10%.

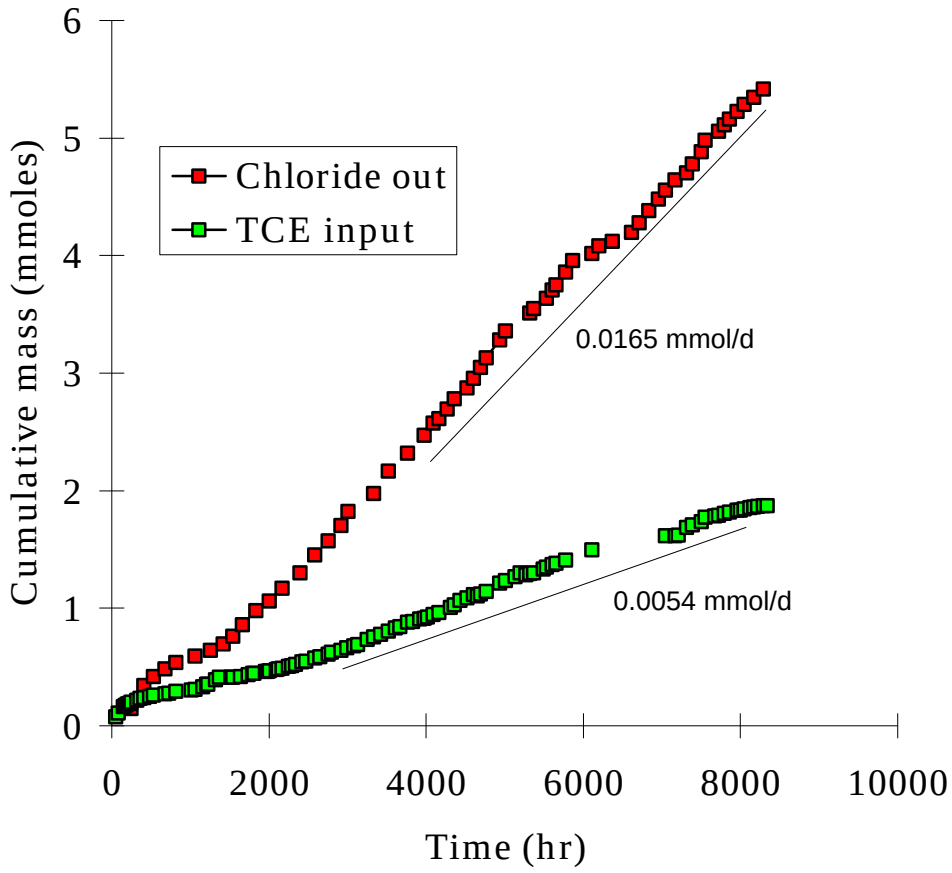

Figure H-3. Comparison of TCE input and chloride removal in Experiment 1

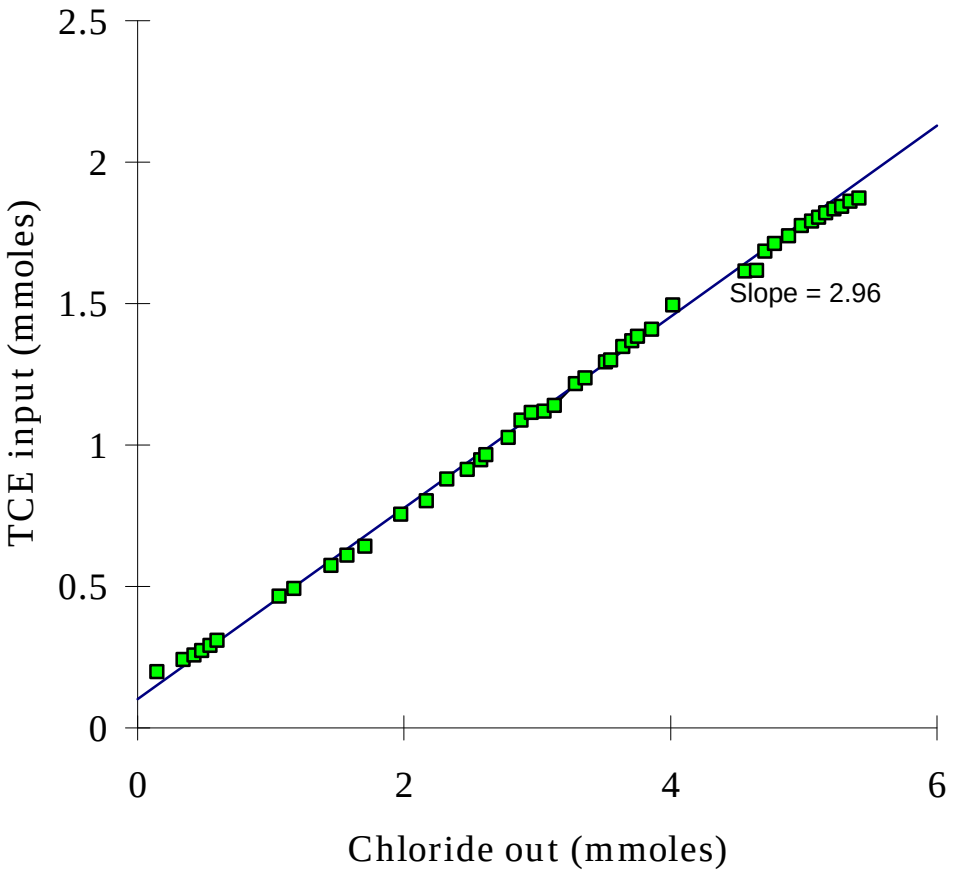

Figure H-4. TCE input vs chloride removed in Experiment 1.

Experiment 2. Fine iron

Because several of the envisioned installation techniques for treatment zones involve pumping a slurry of iron and clay into the ground, there may be rheological advantages to using fine iron to form a slurry. Experiment 2 examined the effectiveness of smaller size iron particles in a treatment zone. The iron was acquired from VWR, and the particle size was less than 40 mesh, or less than 0.015-inch diameter. As in Experiment 1, the iron comprised 20% by weight of the clay slurry. The cumulative effluent vs time is shown in Figure H-5. The applied voltage was initially 10 V and the sample length was 12 cm. After approximately 1,500 h, the applied voltage was increased to 20 V and the flow rate increased. The increase in flow rate was not quite linear with voltage. For the first 1,500 h, the apparent electro-osmotic permeability was 5.0 10^{-6} $cm^2/V/s$; after the voltage was increased, the electro-osmotic permeability was 3.8 10^{-6} $cm^2/V/s$. Approximately 400 h into the experiment, the cell was turned off for 264 h. When the voltage was reapplied, the flow rate returned to its previous value.

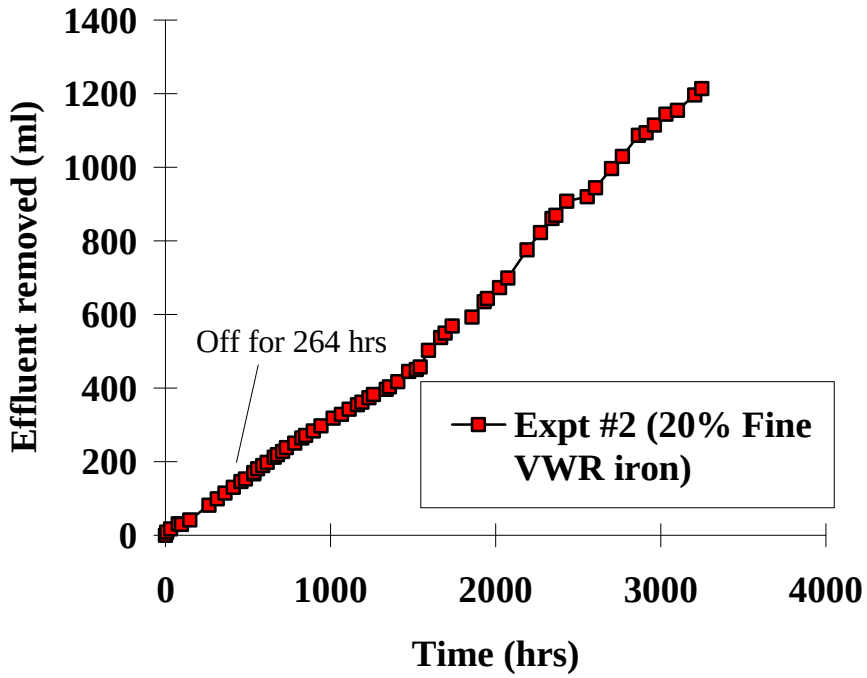

Figure H-5. Cumulative effluent in Experiment 2.

A comparison of the mass of chloride removed in the purge solution to the mass of TCE input into the cell in Experiment 2 is shown in Figure H-6. The average rate of chloride removal after 2,000 h was 0.018 mmol/d compared to the average rate of TCE input, 0.0067 mmol/d. The ratio of these rates is 2.7 mol chloride per mol TCE, or 90% of the stoichiometric ratio of 3 for complete dechlorination. Given the uncertainty associated with chemical analysis and flow rate measurement, the 10% difference is within experimental error. The measurement of the low TCE concentration in the effluent is consistent with nearly complete dechlorination of TCE. The cumulative amount of TCE removed in the effluent is compared to the TCE input in Figure H-7. The TCE concentration in the feed solution was typically in the range of 75 to 90 ppm; the TCE measured in the effluent was always less than 1 ppm. While the effluent chamber was not designed to be gas tight (hydrogen evolving from the cathode must be vented) and loss of some TCE in the effluent is possible, the agreement between the chloride mass balance and the TCE removal suggests that the long-term performance of the iron/clay treatment zone is excellent.

To compare the longevity of these bench-scale experiments to what would be realized in the field, it is best to consider how much water and TCE passed through the treatment zone. In Experiment 2, 60 ml of pore liquid passed through each square centimeter of treatment zone. This liquid carried 3.7 X 10^{-3} mmol of TCE though each square centimeter of treatment zone. The iron loading in the 2.5 cm thick treatment zone was approximately 24 mmol/cm^2. In the field, the expected superficial velocity of the pore water is approximately 0.5 cm/day. On the basis of water volume, Experiment 2 indicates that the treatment zone should perform well for at least 120 days, with no sign of decrease in performance. On the basis of iron available for dechlorination, in Experiment 2 there are 650 mol iron in the treatment per mol of TCE that entered the zone. Depending on the chemical pathway of the TCE dechlorination, the stoichiometric ratio of iron to TCE is 2 to 6 mol/mol. Thus there is a great excess of iron, based

on TCE mass. In fact, the oxidation of iron in water will most likely be the reaction limiting the iron's usefulness. The corrosion of iron in water in discussed below.

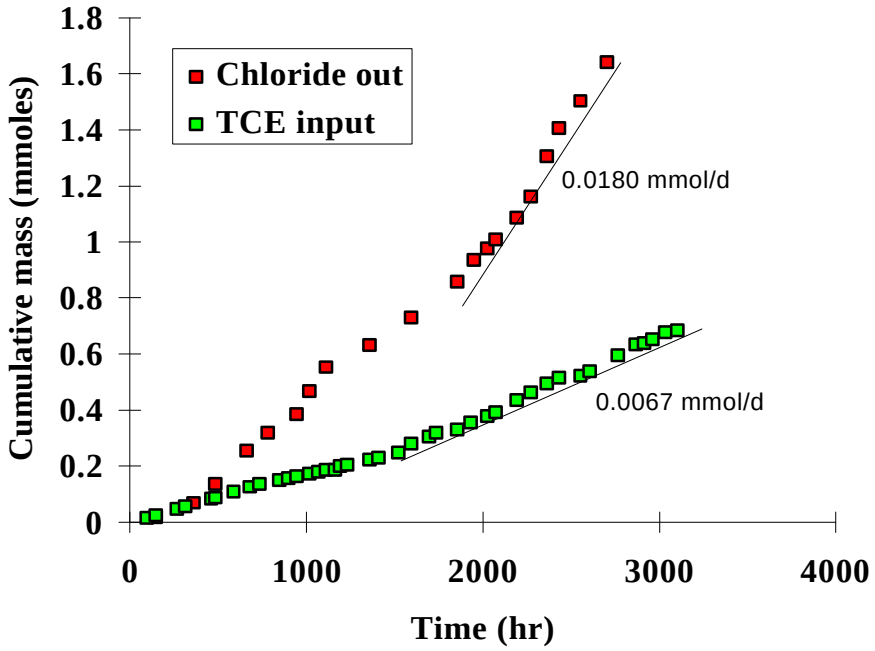

Figure H-6. Comparison of TCE input and chloride removed in Experiment 2.

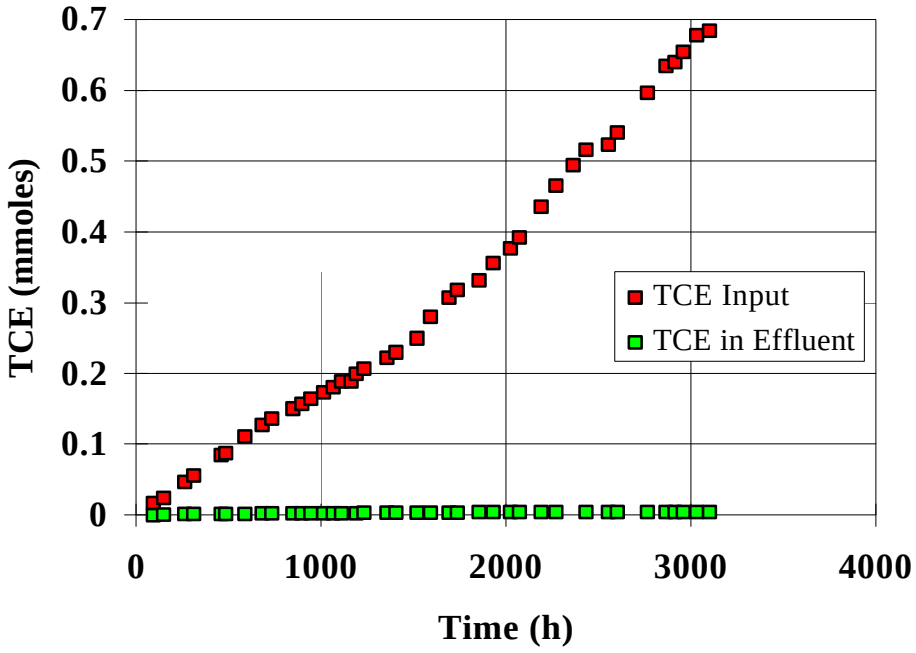

Figure H-7. Cumulative input and output of TCE in Experiment 2

Experiment 3. Paducah model

Based on laboratory tests and price and availability of materials, the treatment zone recipe for Phase IIa was determined to be 29% Peerless fine iron, 35%Thiele kaolin, and 35% water (w/w). The design thickness of the zone was 5 cm. The electrodes were specified to be a mixture of 50% Peerless fine iron and 50% Loresco SWS coke. Once the treatment zone and electrodes construction was specified, a laboratory test cell, Experiment 3, was assembled to model the Phase IIa field test. The purpose of this test was to verify the long-term performance of the materials used in the field in an accelerated experiment.

The cumulative effluent vs time for Experiment 3 is shown in Figure H-8. Twenty volts was applied to the cell, and the length of the clay column was 13 cm. A very steady flow rate was observed for the first 3,000 h. The apparent electro-osmotic permeability during this period was 6.6×10^{-6} cm^2 $V^{-1}s^{-1}$. Over the next 3,000 h, the flow gradually decreased, so that between 5,000 h and 5,500 h the apparent permeability was 2.6×10^{-6} cm^2 $V^{-1}s^{-1}$.

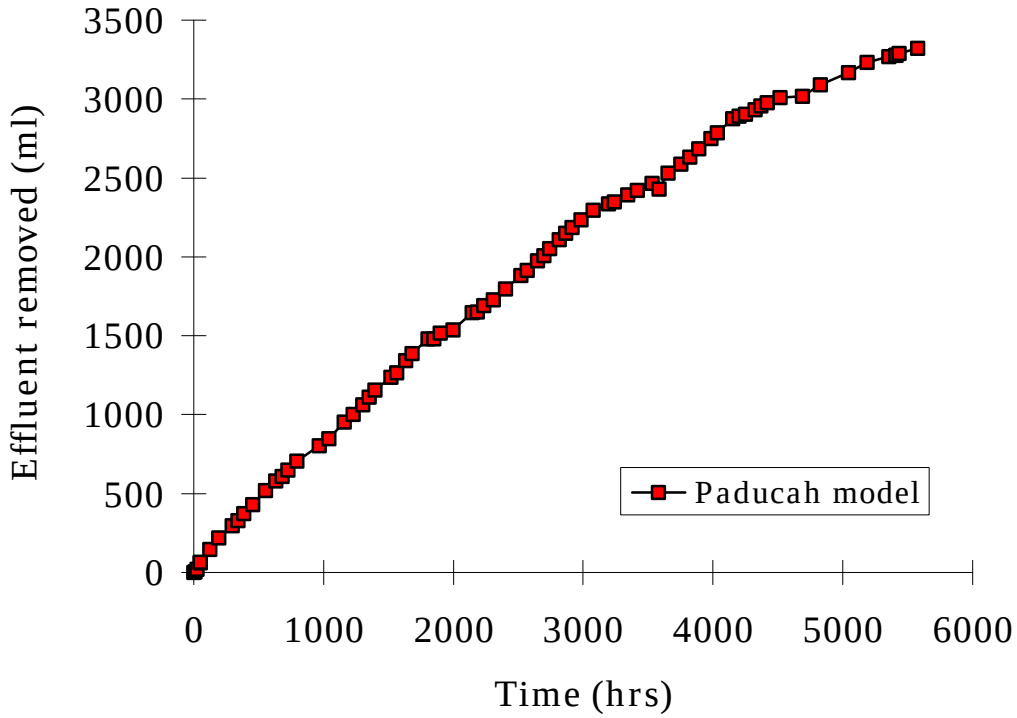

Figure H-8. Cumulative effluent in Experiment 3, the Paducah model.

The comparison of TCE input and chloride collected at the purge reservoir is shown in Figure H-9. As in the previous two experiments, there is excellent agreement between the moles of chloride collected and the amount of chloride that enters the cell in the TCE molecules. The ratio of 3.1 moles chloride per mole of TCE is within the expected 10% experimental uncertainty. This result is very encouraging in terms of the long-term performance of the treatment zones and electrodes used in Phase IIa. Also plotted in Figure H-9 is the volume of pore liquid that passed through the treatment zone. Sixteen hundred L m^{-2} (160 ml cm^{-2}) represents at least 320 days of flow in the field, at the expected flow rate of 0.5 cm d^{-1}. The amount of TCE entering the treatment zone was approximately 0.12 mmol per square centimeter. Because the treatment zone in Experiment 3 is twice as thick as those used in Experiments. 1 and 2, the iron loading per unit cross sectional area is twice as much, or approximately 48 mmol cm^{-2}. Thus, there are approximately 400 moles of iron for each mole of TCE that entered the treatment zone. Given the excellent chloride mass balance, this amount of iron appears sufficient for long-term performance. It must be noted, however, that if the TCE in the pore water were at saturated levels, or approximately 1,100 ppm, more iron would be expected to oxidize. Fortunately, the corrosion rate of iron in water, as discussed below, should dominate the iron consumption, so that even a ten-fold increase in TCE concentration would not be expected to significantly affect the overall rate of iron consumption, and the treatment zone designed for Phase IIa should perform well for long periods of time, even under saturated conditions.

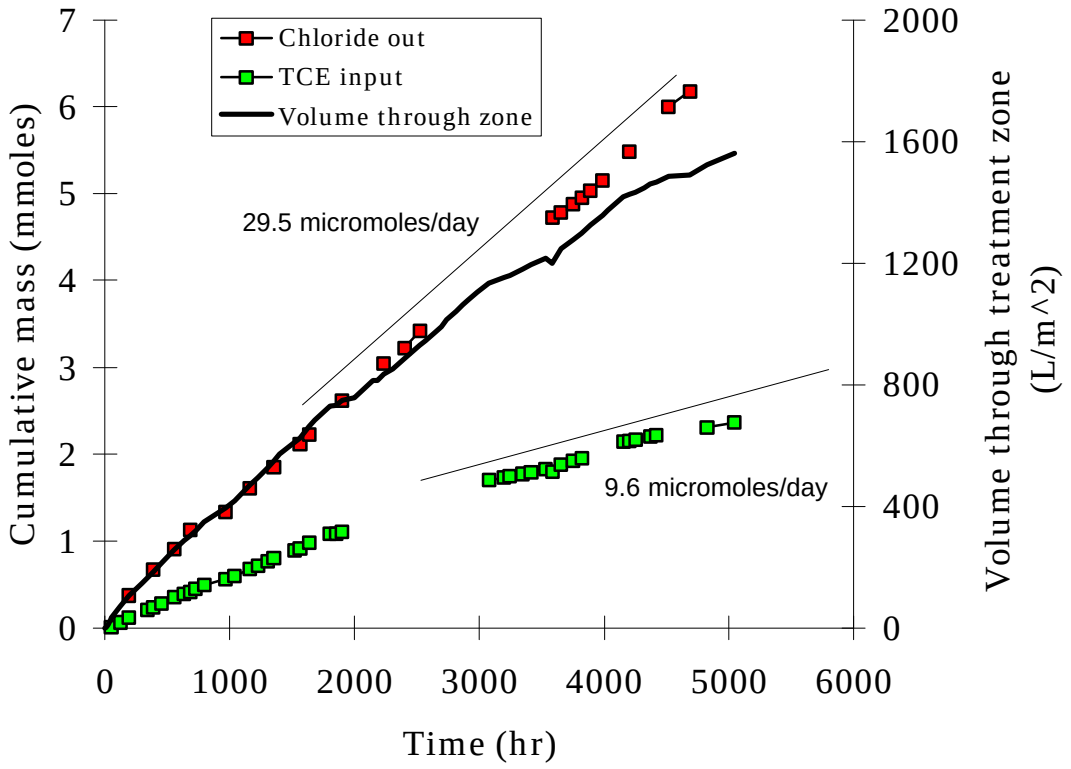

Figure H-9. Comparison of chloride removed and TCE input in Experiment 3, the Paducah model; also plotted is the volume of pore liquid passed through the treatment zone.

Experiment 4. No iron zone I

Economic analysis of the *Lasagna*™ process has indicated that installation of the treatment zones accounts for a major fraction of the overall cost. In addition, recent research has indicated (Klausen *et al.1995*, Sivavec and Horney, 1995,1997) that naturally occurring minerals in contact with ferrous ions can promote dechlorination of halogenated organics. These facts motivated Experiment 4, which consisted of a column of soil from the Paducah site, and did not incorporate an iron treatment zone. Iron was used as the anode and provided ferrous ions to the soil column via the electrochemical reaction $Fe^0 \rightarrow Fe^{+2} + e^-$. The ferrous ions generated at the anode migrate into the soil under the influence of the electric field. The ferrous ions are adsorbed to the soil minerals to some extent, and potentially form a reactive site for TCE dechlorination. The objective of this experiment was to determine if dechlorination of TCE could be achieved by the electrochemical introduction of ferrous ions into the soil.

The cumulative amount of effluent collected in this experiment is shown in Figure H-10. The applied voltage was 20 V and the soil sample was 13 cm long. The initial electro-osmotic flow was relatively high with an apparent electro-osmotic permeability of 4.5 X 10^{-6} $cm^2V^{-1}s^{-1}$. After approximately 1,000 h, the flow rate decreased to a stable rate that represented a permeability of 1.4 X 10^{-6} $cm^2V^{-1}s^{-1}$.

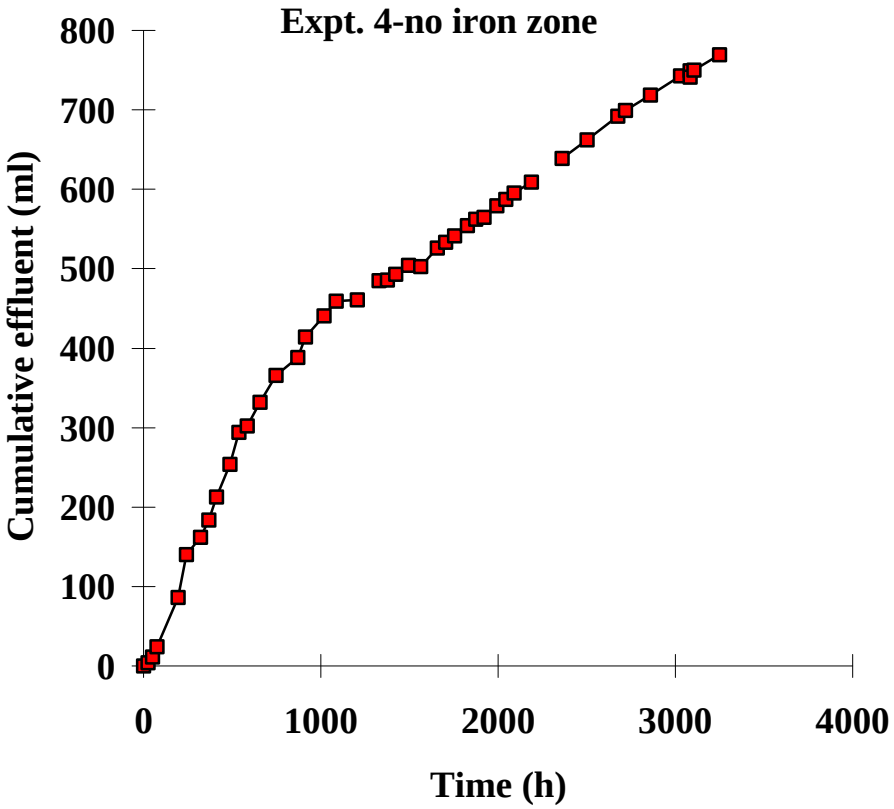

Figure H-10. Effluent vs time for Experiment 4; no iron zone. One pore volume is approximately 101 ml.

A comparison of the TCE input and chloride removed for Experiment 4 is shown in Figure H-11. After approximately 1,000 h, the rate of chloride removal and TCE input stabilized. At this point the rate of chloride removal was 7.3 μmoles/d, compared to the TCE input rate of 2.9 μmoles/d. These results suggest that after an initial transient period, a steady-state performance was achieved in which approximately 84% of the TCE entering the soil column was reduced.

While the chloride mass balance is encouraging, and suggests that native soil may be converted into treatment zones for TCE, the mass balance does not indicate where in the soil column the reduction took place. Extraction of the soil column after the experiment revealed a uniform TCE distribution of approximately 6 to 8 ppm in the soil, as shown in Figure H-12. The pore water is estimated to be 5 times higher than the soil concentration, based on negligible adsorption, a soil density of 2.0 g cm^{-3}, and a porosity of 40%. The pore water remaining in the soil had approximately 30 % of the feed solution TCE concentration (nominally 100 ppm).

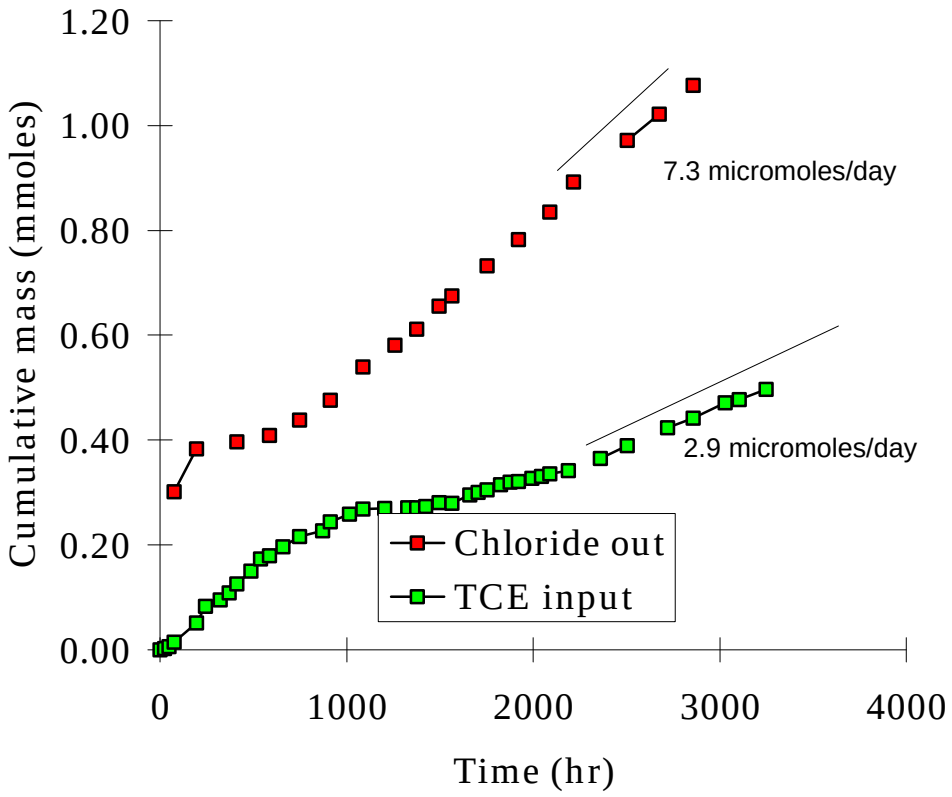

Figure H-11. Cumulative mass of TCE input and chloride removed in Experiment 4.

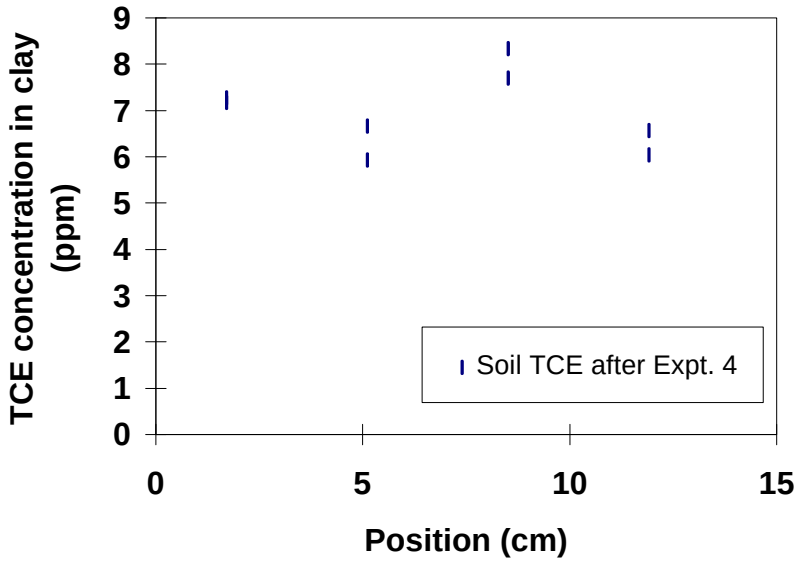

Figure H-12. TCE distribution in soil column after Experiment 4.

Experiment 5. No iron zone II

Experiment 4 was repeated to verify the degree of dechlorination achieved without an iron zone and to verify TCE distribution in the clay column at the end of the test. Because of the possibility that the dechlorination observed as chloride in the purging liquid in Experiment 4 was actually produced at the cathode instead of in the soil column, a modification was made to the experimental apparatus. A cation exchange membrane was added between the clay sample and the cathode reservoir to prevent chloride produced at the cathode from migrating back toward the anode, where it would be removed with the purging liquid.

The cumulative amount of effluent collected in this experiment is shown in Figure H-13. The applied voltage was 30 V and the soil sample was 12.7 cm long. The majority of the voltage drop occurred in the electrode chambers. The effective electric field, as determine by the gradient measured within the clay sample, was 0.21 V cm^{-1}. After an initial period of no apparent flow, the initial electro-osmotic permeability was approximately 3.5 X 10^{-6} $cm^2V^{-1}s^{-1}$. This permeability was constant for the remainder of the 4,000 h test.

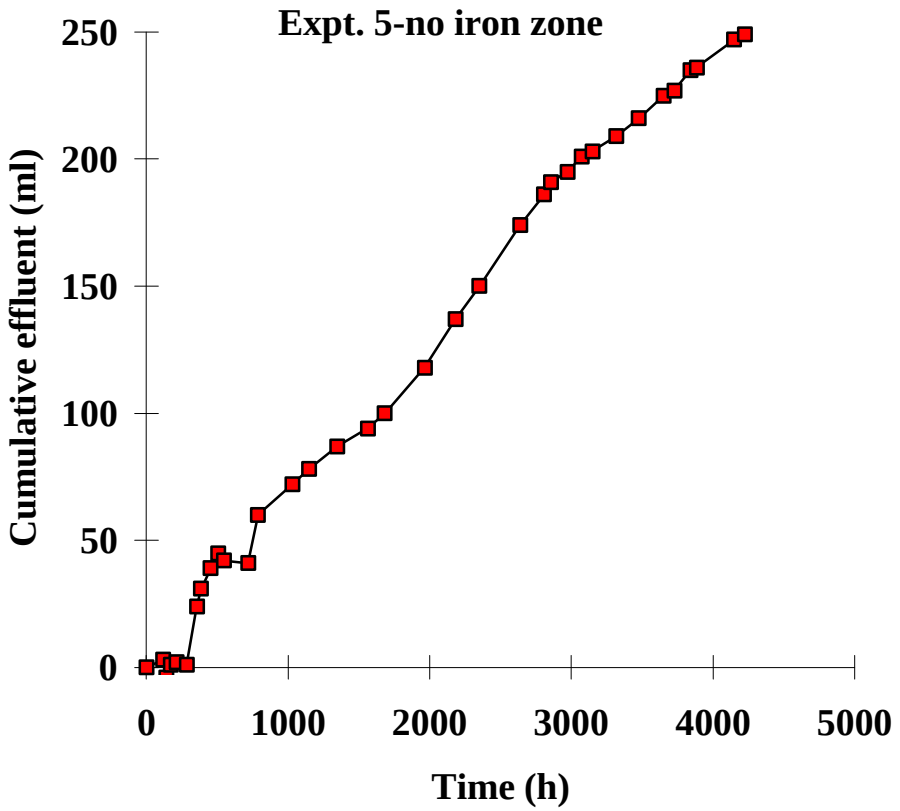

Figure H-13. Effluent vs time for Expt. 5; no iron zone. One pore volume is approximately 99 ml.

A comparison of the TCE input and chloride removed for Experiment 5 is shown in Figure H-14. After approximately 1,500 h, the rate of chloride removal and TCE input stabilized. At this point the rate of chloride removal was 5.7 µmoles/d compared to the TCE input rate of 1.8 µmoles/d. These results suggest that after an initial transient period, a steady-state performance was achieved in which 105% of the TCE entering the soil column was reduced. The accuracy of

these measurements is probably no better than +/- 10 %. This result is very encouraging for the prospect of creating a reactive soil zone using an iron anode.

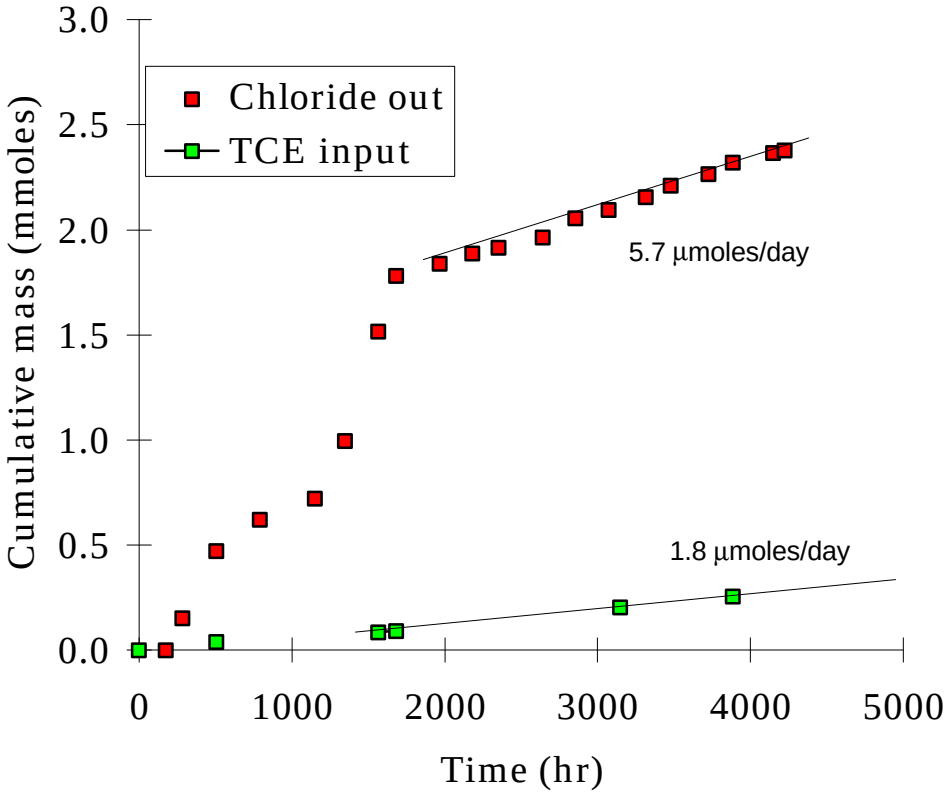

Figure H-14. Cumulative mass of TCE input and chloride removed in Expt. 5.

The distribution of TCE remaining in the soil is shown in Figure H-15. Two cores were taken from the soil sample and sectioned into 3.2 cm lengths, providing duplicate samples to characterize each location. The TCE was extracted from the samples by agitation in mixture of water and hexane overnight. After allowing the hexane and water phases to separate, the hexane was analyzed using GC/EC for TCE detection. In this experiment there is an apparent decrease in TCE concentration as the pore water moves through the soil column. The reactivity, as evidenced by the change in slope of the concentration distribution, appears to increase nearer the cathode. This distribution suggests that the dechlorination was taking place within the soil, as opposed to at the cathode. If the reaction were taking place at the cathode, the concentration distribution would be nearly uniform in the soil column. It should be noted that the pore water is not at the expected concentration of approximately 100 ppm. It is approximately 33 ppm at the anode side of the column. It is therefore possible that a significant amount of TCE is lost in the process of taking the cell apart and extracting the TCE. However, if we assume that the efficiency of the coring and extraction process is the same for all samples, then the actual distribution would have a similar shape to the one shown in Figure H-15, except the concentrations would be approximately three-fold higher.

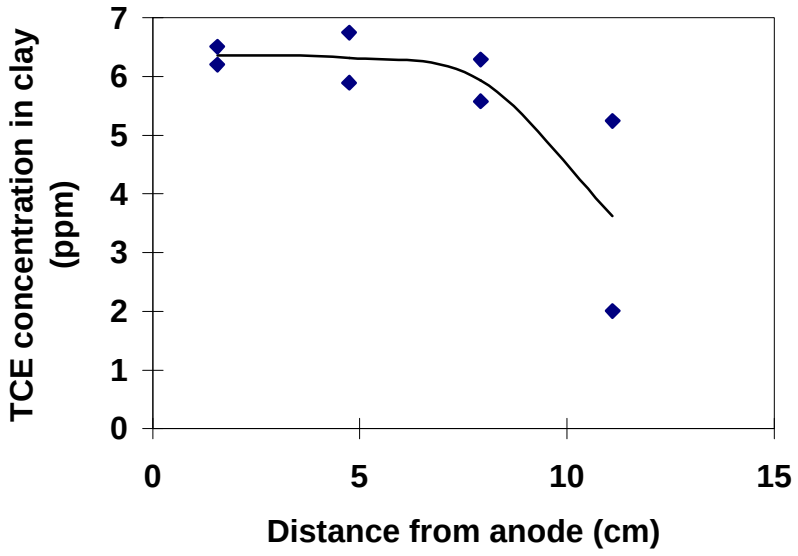

Figure H-15. TCE distribution in soil column after Expt. 5.

Summary

Several experiments were conducted to evaluate the long-term performance of iron/kaolin treatment zones in the *Lasagna*™ process. The results are very encouraging. In all cases, a mass balance between TCE input into the cells and chloride ions removed showed essentially complete dechlorination of the TCE to within approximately 10% experimental error. While the laboratory tests mimicked field conditions, they were performed at room temperature. Previous tests (Topical Report, Task 9, Phase I) have shown that elevated temperatures encountered in the field would increase the dechlorination reaction rate, and therefore the laboratory results provide a conservative estimate of what would happen in the field. The tests were run for enough time and pore volumes to allow the conclusion that the iron/kaolin treatment zones installed in the Paducah field test should last at least 320 days without signs of degrading performance. Calculations indicate that for the pore water containing 100 ppm TCE, the treatment zones installed in Paducah have approximately 100 times the iron required to last 320 days. Even if the pore water were saturated with TCE (1,100 ppm), there would be enough iron to last several years.

Experiments conducted without iron treatment zones are very intriguing. When using iron as an anode to electrochemically inject ferrous ions into the soil, dechlorination of 84% of the TCE was determined by measuring chloride removed from the system. Because the ferrous ions move faster than the pore water flow from electro-osmosis, it is possible to create reactive zones which destroy most of the TCE in situ before it is convected to the cathode. The TCE that reaches the cathode will be electrochemically reduced. This concept has the potential to greatly reduce to cost of remediation by eliminating treatment zones.

I. Bipolar Electrode Effect

The bipolar electrode effect occurs in systems in which current is carried by both ions and electrons. In the *Lasagna*™ process, iron metal in the treatment zone saturated with ground water can behave as a bipolar electrode. The externally applied electric field acts on ions in the pore water and electrons in the metal particles. Depending on the local electric field strength acting on the iron surface, two possible scenarios occur: At low field strength, electrons form a negative charge on the surface of the particle closest to the anode, and a complementary positive charge develops on the surface closest to the cathode. These surface charges are balanced by a charged double layer in the solution. The thickness of the double layer is on the order of 10 nm and, if the voltage drop across the double layer is below the level required for electrochemical reactions to occur (approximately 0.8 V for water), then no current flows through the iron particle. If the applied electric field is increased, then the voltage drop across the double layer can be higher than the electrochemical stability threshold. Under these conditions, Faraday reactions will occur at each end of the metal particle. These electrochemical reactions transfer charge from the ions in solution to electrons in the metal. The net effect of these reactions in aqueous systems is that the side of the metal facing the anode behaves as a cathode, generating OH^- by the electrolysis of water. The other end of the metal behaves as an anode and will generate ferrous ions under normal conditions. If the metal were more noble, electrolysis of water could occur on the anode side generating H^+. In a system comprised of a packed bed of iron particles, the overall behavior is dependent on the interparticle contact because large particles will have a bigger potential drop across the double layer than smaller particles in the same applied electric field. Therefore experiments have been conducted to investigate the behavior of a packed bed of iron particles in an electric field.

Experimental methods

The test cells were cylindrical glass columns (20 cm x 5 cm dia.) similar to those shown in Figure H-1. Instead of loading the cell with clay, agar gel was used as the porous medium. The advantage of agar is that it is transparent and highly porous (>98%). This enables pH-indicating dyes to be used to monitor the development and propagation of pH fronts from the electrodes and the iron treatment zones. No TCE was used in these experiments because its effect on the electrochemistry of the iron water system should be negligible. Agar was mixed with 0.001 M aqueous solution of sodium sulfate at a ratio of 1:50 by weight. The mixture was heated to approximately 60°C to dissolve the agar, and the solution was poured in the glass columns to gel. A feed solution containing pH-indicating dye was fed into a chamber at the anode side of the cell. Electro-osmosis drove some of the feed solution toward the cathode. Enough feed solution was supplied so that some would overflow the chamber so that nearly constant conditions could be maintained in the chamber. The column end caps used to form the catholyte, anolyte, and purging chambers were made from Teflon and sealed using silicone o-rings. Stainless steel rods 0.32 cm in diameter were used to monitor the voltage distribution in the cell. The rods penetrated holes in the glass column and reached the central axis of the column. The voltage probes were sealed at the outside of the column with a gasket compressed by a modified hose clamp.

Experiments were conducted with and without an iron zone so that a comparison of the pH profiles could be made. The observations in the experiments involving the bipolar electrode effect were visual; however, comparisons of the pH front propagation speeds in experiments without a

treatment zone compared well with computer modeling developed in Phase I. The comparison of experiments and model calculation was presented in Topical Report for Tasks 2-4 for Phase I.

In addition to the agar experiments, one of the long term experiments with clay and an iron/kaolin treatment zone was dissected to measure the pH distribution. This experiment, labeled Experiment 3 (the Paducah model in Section 2.2) showed long-term excellent dechlorination efficiency from the iron zone.

Results and Discussion

Photographs of the agar cells before and after application of voltage are shown in Figures I-1 through I-4. The pH-indicating dyes turn red at low pH and purple at high pH. Without an iron zone in the cell, a single low pH front can be observed to propagate from the anode. This low pH results from the production of H^+ from water electrolysis at the platinum anode and subsequent ionic migration of the acid toward the cathode. A high pH front is observed propagating from the cathode where electrolysis of water produces OH^-, which migrates toward the anode. These fronts are clearly visible in Figure I-2.

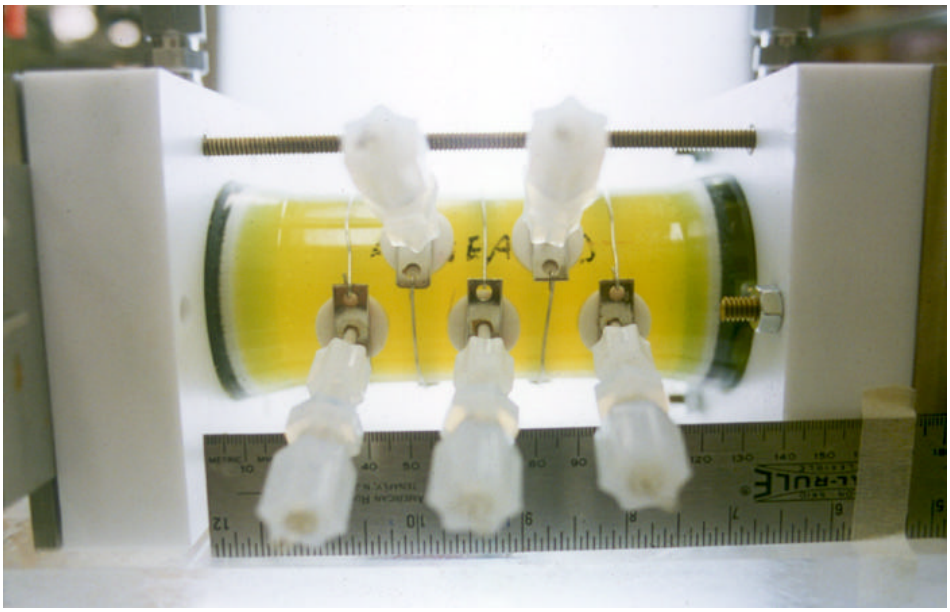

Figure I-1. Photograph of agar experiment without iron zone. Anode is on the left and cathode on the right.

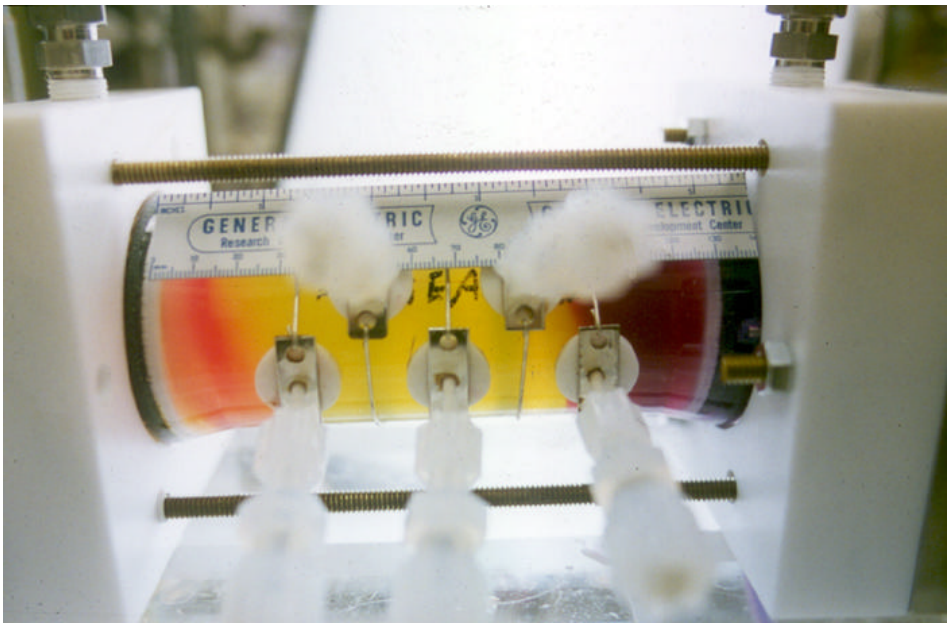

Figure I-2. Photograph of agar experiment without iron zone after application of 20 V for 1 h. Red color indicates low pH and purple indicates high pH.

The experiment with the iron zone shows two high pH fronts developing in the cell (Figure I-4). One emanates from the cathode as in the previous experiment. The other high pH front emanates from the side of the treatment zone facing the anode. Thus, the electrochemical reactions are induced on each side of the treatment zone by the applied field. The reason a low pH front is not visible on the cathode side of the treatment zone is that instead of electrolysis of water, which occurs at the anode and produces H^{+}, corrosion of the iron releases Fe^{+2} ions into solution. The ferrous ions migrate to the cathode; however, they do not cause a large enough pH change to alter the dye color.

These experiments clearly show the presence of electrochemical reactions induced in the treatment zone material by an applied electric field. While the effect of these reactions on the dechlorination of TCE was not studied in these experiments, it has been demonstrated by Monsanto that dechlorination does occur at cathodes. Therefore it is plausible that the bipolar electrode effect may enhance the dechlorination rate of the iron.

Figure I-3. Photograph of agar experiment with iron zone. Anode is on the left and cathode on the right.

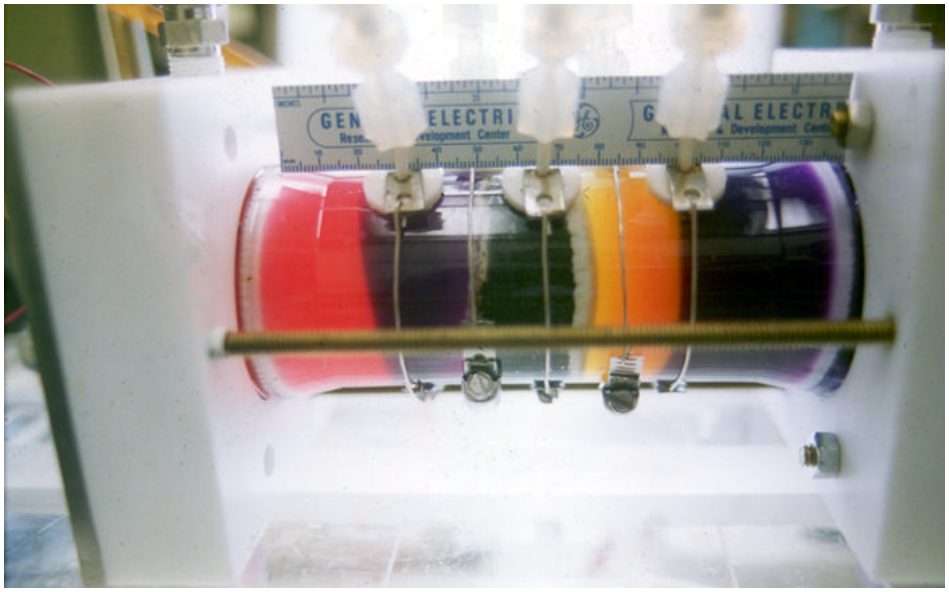

Figure I-4. Photograph of agar experiment with iron zone after application of 20 V for 1 h. (Red color indicates low pH and purple indicates high pH. Purple color emanating for left side on iron zone indicates electrochemical generation of OH^- via the bipolar electrode effect. Dissolution of ferrous ions on the right side of the iron zone do not alter the pH or color of the agar.)

The final experiment investigating the bipolar electrode effect addressed the iron/clay treatment zone used in long-term Experiment 3, reported above in Section H. In this experiment the pH distribution in the column was measured after approximately 8,000 h of operation, during which the treatment zone dechlorinated the input TCE with high effectiveness. This pH distribution is shown in Figure I-4. This experiment with an actual iron/clay treatment zone was operated for 1 year in contact with soil from the Paducah field site shows that the bipolar electrode effect does not significantly affect the pH near the treatment zone. The reason is that

the pH buffering capacity of the soil effectively neutralizes the pH fronts that emanate from the electrodes as well as those that originate at the iron zone edges. It should be noted, however, the data presented in Figure I-5 do not suggest that electrochemical reactions are not occurring at the treatment zone edges. The data simply indicate that any such reactions have negligible effect on the soil pH.

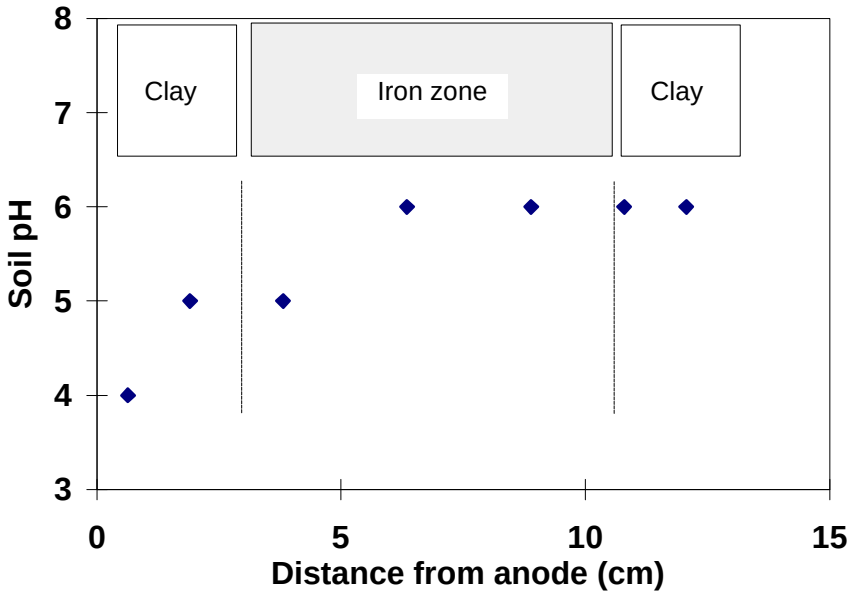

Figure I-5. pH distribution in Experiment 3 form Section 2.2 after 8,000 h of operation. Anode chamber was to the left, cathode to the right.

J. Movement of DNAPLs in Electric Fields

Introduction

In many potential applications of the *Lasagna*™ process, there is a high likelihood of TCE existing as a Dense Non-Aqueous Phase Liquid (DNAPL) in the soil at some sites. Monitoring of the water well TCE concentrations and carbon cassettes in Phase IIa indicated the presence of DNAPL at the Paducah site. Several experiments were conducted to investigate the mobility of non-aqueous phase TCE in an electric field.

Experimental methods

The experiments presented in this section were conducted in columns similar to those used in the long-term experiment in section H. Experiments 1through 5 were presented in that section. In this section, Experiments. 6 through 9 are presented. Experiments 6 through 8 examined the migration of non-aqueous phase TCE in saturated clay without the presence of an iron treatment zone; Experiment 9 examined the migration of non-aqueous phase TCE in a saturated clay column with an iron treatment zone. Experiment 6 used a glass tube with an internal diameter of 5/16 in. (0.80 cm) and Experiments 7 and 8 used a glass tube with an internal diameter of 0.5 in. (1.3 cm) for a column. In both experiments the columns were packed with a mixture of Thiele kaolin and 0.001 M Na_2S0_4 in water (60:40 weight ratio). Flexible tubing connected to the ends of the glass tube were bent to form a 90° curve, in effect creating a U-tube geometry for the cells. The flexible tubing functioned as the electrode chambers, and gas generated from the electrolysis of water could bubble out the top. Platinum wires were used as electrodes. The flow rate was determined every day by the changes in liquid levels in both branches of the U-tube. Good agreement between the changes in liquid levels of the anode and cathode chambers indicated the water loss via evaporation and electrolysis was negligible.

In Experiment 6, a small batch of the kaolin mixture was combined with neat TCE to form a mixture with a TCE concentration of 3,500 ppm. Neglecting TCE adsorption to the clay, the pore space should have approximately a five-fold higher concentration than the soil as a whole. Therefore the expected pore water concentration was approximately 1.8% TCE, or well above the saturation level of 1,100 ppm. A hydrophobic dye, Sudan IV, was added to the TCE-containing mixture to create pale purple coloring of the clay. The purpose of the dye was to enable detection of the motion of the neat TCE phase through the clay. The glass tube was first packed with a 7.3-cm section of the TCE-free kaolin mixture; 5.7 cm of the TCE/kaolin mixture was then packed adjacent to the first section. Finally 7.0 cm of the TCE-free kaolin mixture was packed adjacent to the TCE-containing section, thus making a column of clay in which the TCE-containing section was surrounded by sections of clay devoid of TCE. Ten volts was applied to the column for 7 days. The apparent electro-osmotic permeability was 1.7 X 10^{-5} cm^2 $V^{-1}s^{-1}$. Over the 7-day period, the pore liquid moved 13 cm through the clay.

Experiments 7 and 8 were essentially repeats of Experiment 6 with modifications made to limit potential losses of TCE. In this experiment a larger diameter glass tube was used for the column. The 1.3-cm diameter tube was 15.2 cm long and had a port attached to the side to permit injection of neat TCE into the packed clay column. A diagram of this column is shown in Figure J-1. No dye was used in this experiment. In Experiment 7, a column of kaolin clay (40% water by weight) 15 cm long was loaded in the apparatus. Electro-osmosis was driven with an applied voltage of 20 V for 3 days with no TCE in the system. On the third day, 22.6 µL (33

mg) of TCE was injected into the port on the column, and the applied voltage was reduced to 10 V. For comparison, this amount of TCE, if distributed uniformly through a 2.5-cm section of clay, would yield a concentration of 5,000 ppm based on wet clay weight, over 20 times saturation levels.

In Experiment 8, a 15-cm long column of kaolin clay (40% water by weight) was loaded into the apparatus shown in Figure J-1. Ten volts was applied to the platinum electrodes for 3 days before 20 μL (29 mg) of TCE was injected into the side port on the column.

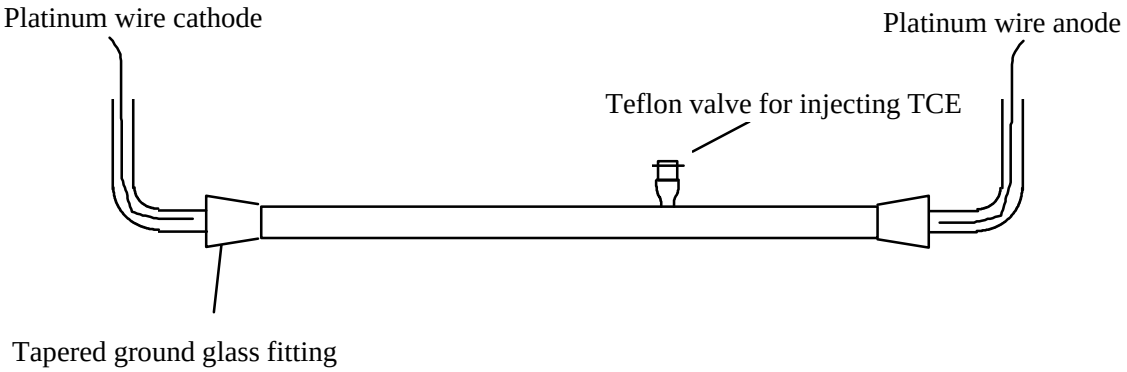

Figure J-1. Schematic of apparatus used in Experiment 7 and 8.

In Experiment 9, the performance of iron treatment zones was investigated with non-aqueous phase TCE. The construction of the test cell is shown in Figure J-2. A 5.0-cm diameter glass column was used for this experiment. Thiele kaolin and 0.001 M Na_2S0_4 in water (60:40 weight ratio) was loaded into the cathode end of the column to form a 3.5-cm section of clean clay. Adjacent to this clean region on the anode side was the 3.5-cm thick iron/kaolin zone comprised of 20% (wt) Peerless fine iron and 80% of the Thiele kaolin/water mixture. Another clean kaolin region (3.2-cm thick) was packed on the anode side of the iron treatment zone. Two filter papers were placed on the anode side of this region. After these filter papers were emplaced, the column was put in a walk-in refrigerator at 4°C for 16 h. In the refrigerator 1.1 g of TCE was added to the filter papers before a final layer of clean kaolin, 3.8-cm thick, was placed on the anode side of the filter papers. Carborundum porous stones lined with filter paper were used to confine the column. An apparatus similar to that shown in Figure H-1 was used to conduct Experiment 9.

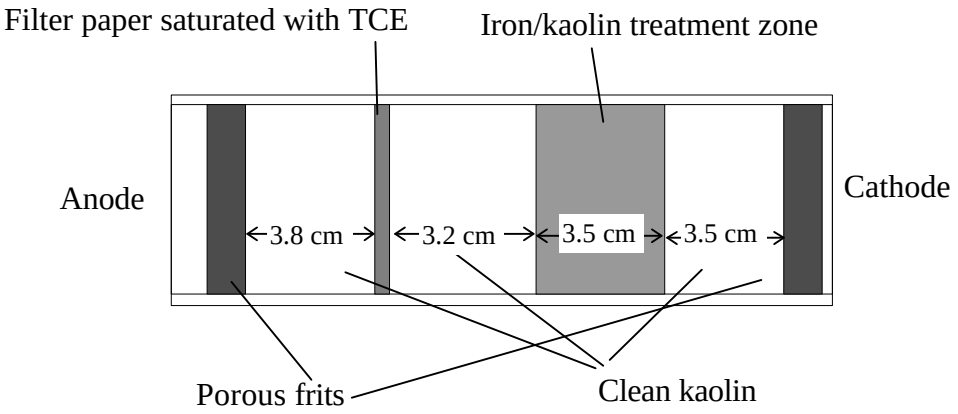

Figure J-2. Schematic of construction of column for Experiment 9.

In Experiments 6 and 9, the initial TCE distribution was established in the construction of the test cell. In Experiments 7 and 8, the initial TCE distribution was determined by injecting a spike of TCE into the middle region of the column. The final TCE distributions were determined, in all cases, by extruding the clay column from the glass tube, sectioning the clay into 2- to 3-cm thick regions, and extracting the TCE in a hexane/water (50:50 by volume) mixture. The ratio of extracting phase to clay weight was approximately 10:1. TCE was measured in the hexane phase using headspace analysis via GC/MS.

Results

Experiment 6. Non-aqueous phase TCE in clay column

The before and after distributions of TCE in Experiment 6 are shown in Figure J-3. The total length of the column was 20 cm. The middle 5.7 cm was spiked with TCE to a concentration of 3,500 ppm. After application of 10 V for 1 week, the pore water moved 13 cm through the clay column. The clay was then sectioned into 2.5-cm regions for extraction of TCE. Based on the distribution shown in Figure J-3, the mean displacement of the TCE was 2.5 cm, or approximately 19% the displacement of the pore water. Clearly some dissolution took place as some to the TCE was detected in the cathode region. The concentration above which non-aqueous phase TCE is expected is approximately 220 ppm. Thus it appears that some of the non-aqueous phase TCE moved approximately 5.0 cm, or 38% as fast as the pore water. Diffusion can account for some dispersion of the TCE profile. Estimating the diffusion length as $(Dt)^{1/2}$ and using 10^{-6} cm^2 s^{-1} for the diffusivity of TCE in clay, diffusion can be expected to move the dissolved TCE approximately 1 cm in one week. Thus molecular diffusion cannot explain the migration of the TCE. In addition, the biasing of the concentration profile in the direction of flow indicated convection of non-aqueous phase TCE. Unfortunately, in this experiment only 13% of the initial TCE is accounted for in the final distribution. Possible sources of error include volatilization of TCE during mixing of the TCE-spiked clay and during loading and sectioning of the clay column. Up to 14% of the TCE may have been removed from electro-osmotic convection of saturated core liquid.

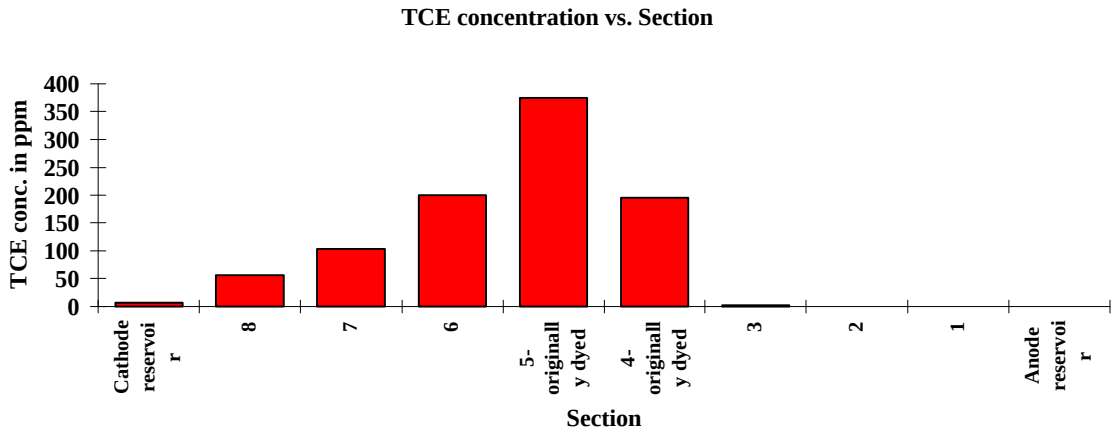

Figure J-3. Comparison of TCE distribution before and after electro-osmosis. Flow was toward the cathode, and each section is 2.5 cm wide.

Experiment 7. TCE spike added to clay column I

Because of the relatively poor mass balance of TCE measured in Experiment 6, a different apparatus, shown in Figure J-1, was used in an attempt to decrease potential losses of TCE to volatilization. The electro-osmotic flow for this experiment is shown in Figure J-4.

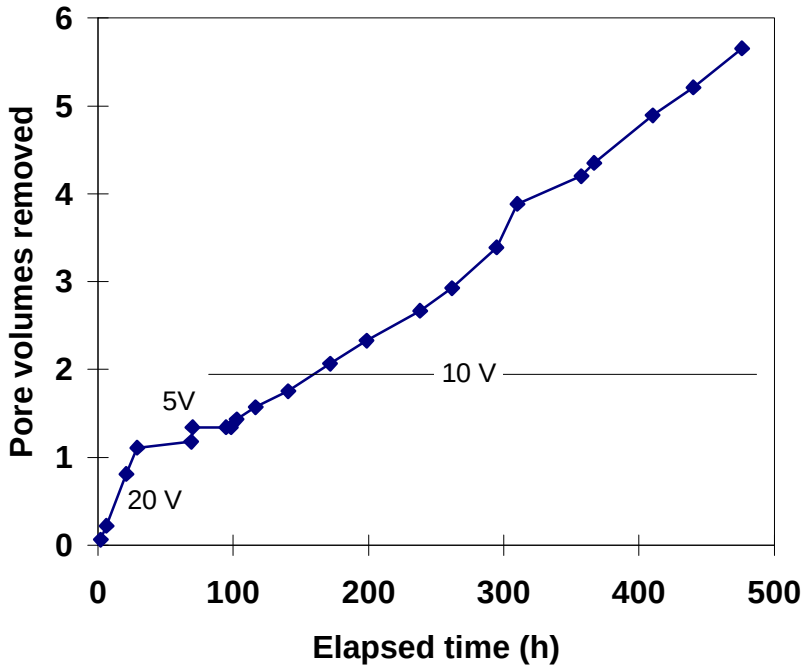

Figure J-4. Pore volumes removed in Experiment 7. 33 mg of TCE injected at 90 h.

In Figure J-5, the distribution of TCE after the experiment is compared to the initial spike of TCE added to the clay column. For plotting purposes, the initial TCE spike was assumed the be uniformly distributed in a 2.5-cm length of the clay column. After the TCE spike at 90 h, 4.3 pore volumes of flow passed through the cell. Based on the analysis of the TCE remaining in the clay, 92% of the TCE was removed. If the TCE were dissolved uniformly in the pore volumes, the concentration would have been 922 ppm, which is near the solubility limit of TCE in water (1,100 ppm).

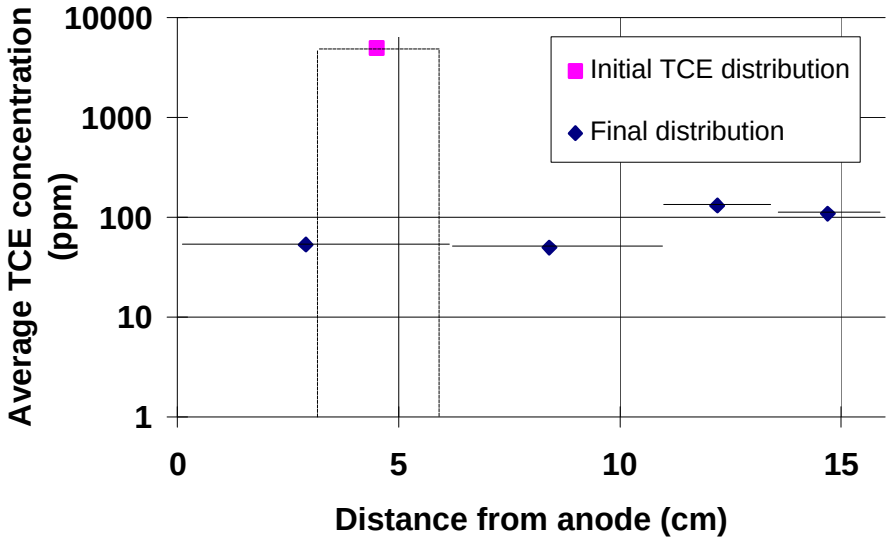

Figure J-5. TCE distribution before and after electro-osmotic purging in Experiment 7. Final TCE remaining in clay accounted for 8% of initial spiked amount.

Experiment 8. TCE spike added to clay column II

To confirm the excellent removal of TCE in its non-aqueous phase state, Experiment 8 was conducted as a repeat of Experiment 7. The electro-osmotic flow for this experiment is shown in Figure J-6.

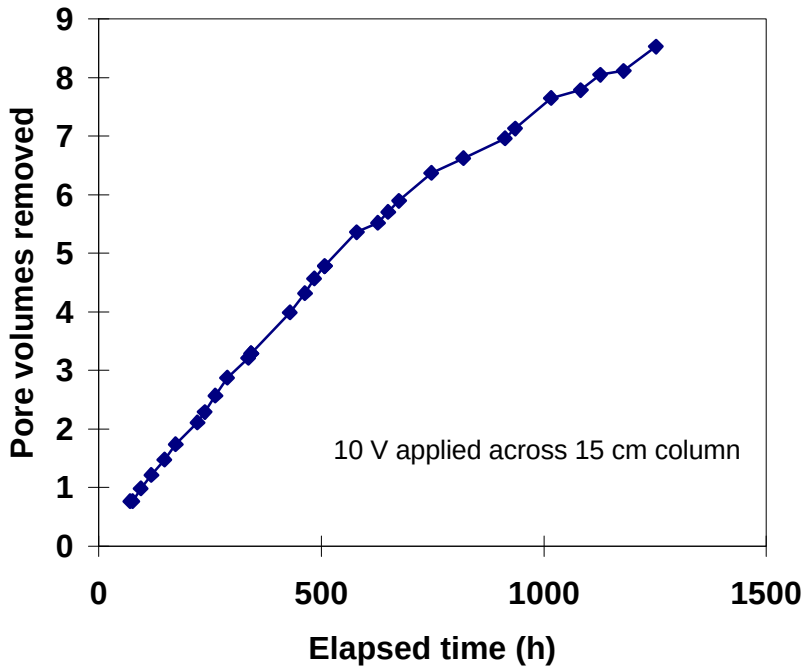

Figure J-6. Pore volumes removed in Experiment 8. 29 mg of TCE injected at 76 h.

In Figure J-7, the distribution of TCE after the experiment is compared to the initial spike of TCE added to clay column. As before for plotting purposes, the initial TCE spike was assumed

to be uniformly distributed in a 2.5-cm length of the clay column. After the TCE spike at 76 h, 8 pore volumes of flow passed through the cell. Based on the analysis of the TCE remaining in the clay, 99% of the TCE was removed. If the TCE were dissolved uniformly in the 8 pore volumes, the concentration would have been 447 ppm. Comparison of Experiments 7 and 8 shows that the additional 4 pore volumes of purging in Experiment 8 reduced the residual TCE to less than 10 ppm. The TCE remaining in the clay in Experiment 7 was an average of 65 ppm. These experiments clearly indicate the effectiveness of electro-osmosis in sweeping high concentrations of TCE out of clay.

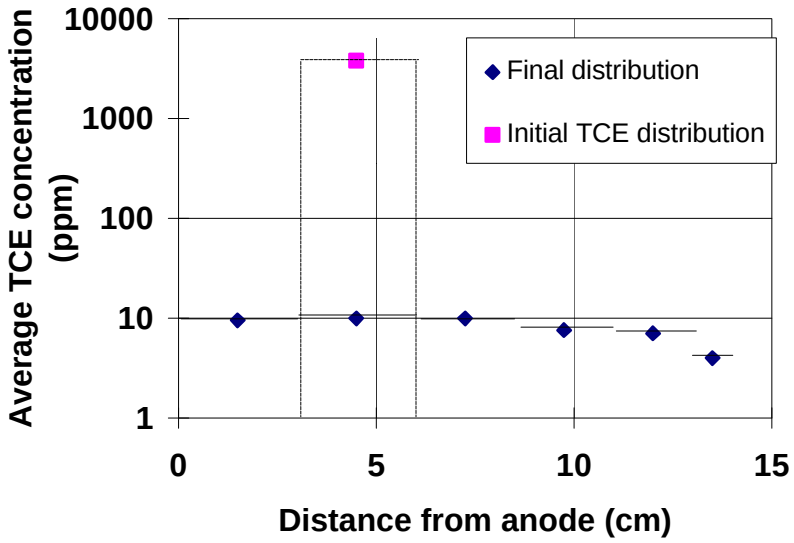

Figure J-7. TCE distribution before and after electro-osmotic purging. Final TCE remaining in clay accounted for 1% of initial spiked amount.

Experiment 9. Saturated TCE with iron zone

The flow rate from electro-osmosis was not consistent in Experiment 9 and caused the test to be terminated after 800 h. The cumulative effluent and current for the experiment is shown in Figure J-8. For the first 80 h, there was a typical flow from anode to cathode. The apparent flow rate dropped for the next 300 h. After 400 h the flow appeared to be going toward the anode. However these flow rate measurements are based on measured volumes of catholyte. It is possible that an undetected leak occurred at the cathode end, resulting in loss of catholyte and erroneous effluent measurements. When the cell was dismantled, a crack in the glass column was observed consistent with the possibility of loss of catholyte. Twenty volts was applied across the 14-cm sample for a average field of 1.4 Vcm^{-1}. If we assume the electro-osmotic permeability was 5.0 10^{-6} $cm^2/V/s$, typical for these experiments, then the superficial velocity was approximately 0.6 cm d^{-1}. This is in good agreement with the measured flow in the first 100 h of the experiment. It seems reasonable that the leak at the cathode occurred at approximately this time.

The cell was divided into sections after chilling to 4°C, and hexane extraction of TCE was performed. The final distribution of TCE is compared to the initial distribution in Figure J-9. It is clear from this distribution that there was migration of non-aqueous phase TCE toward the cathode. It is also apparent that no significant concentration of TCE was measured on the cathode side of the iron treatment zone. The concentration of TCE was 264 ppm in the section

from 3 to 5.5 cm, and 1,180 ppm in the section from 5.5 to 8.5 cm. These high levels are indicative of non-aqueous phase TCE in these regions. The TCE measured in the column after the experiment accounted for 17% of the initial TCE.

The chloride collected in the purge overflow and the anolyte and purge chambers at the end of the test, as shown in Figure J-10, accounted for 76% of the chloride added in the TCE spike. Thus, a total of 93% of the TCE spike was accounted for in either the form of TCE remaining in the clay or chloride collected at the anode region. These results are very encouraging for the application of the *Lasagna*™ process to soils in which non aqueous phase TCE is present. If we assume that the non aqueous phase TCE traveled an average of 5 cm to the middle of the iron zone during the 800 h test, then the TCE was convected at a rate of approximately 10% of the electro-osmotic flow.

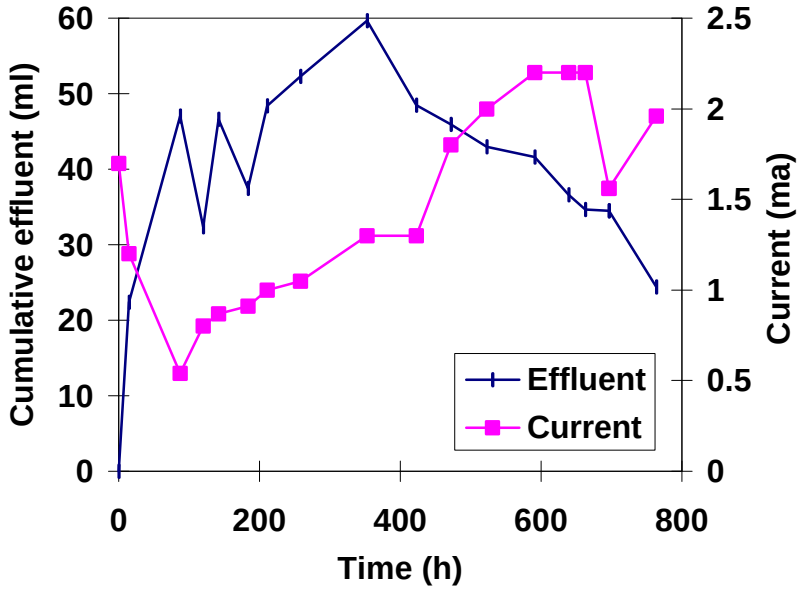

Figure J-8. Cumulative effluent and current in Experiment 9.

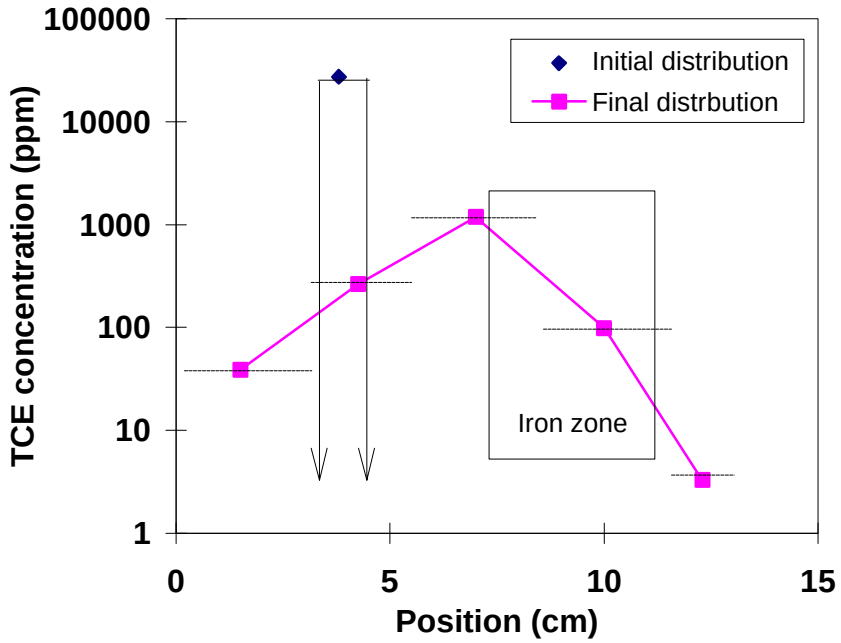

Figure J-9. TCE distribution before and after electro-osmosis.
(Horizontal bars indicate width of section. Anode chamber is at x = 0 cm and cathode is at x = 14 cm. Flow is from left to right. Location of iron zone is indicated by rectangle at 7.5 to 11.0 cm.)

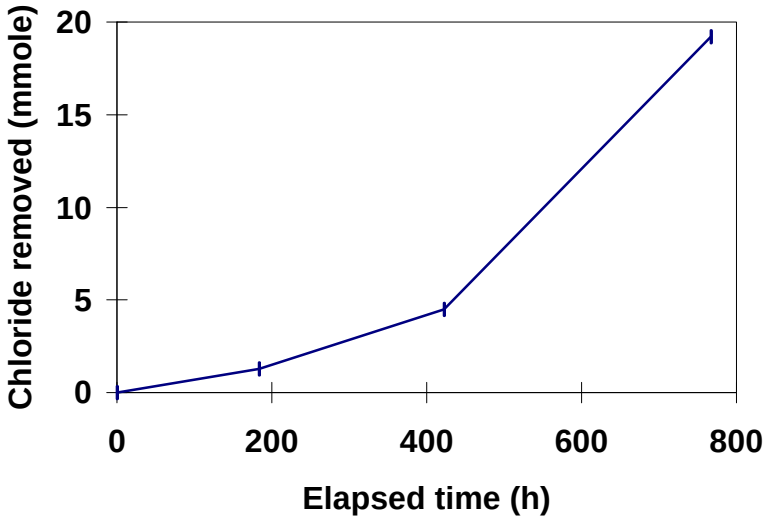

Figure J-10. Removal of chloride of cell in Experiment 8. Initial spike of TCE was 8.4 mmoles, or 25 mmoles of chloride. Nineteen mmoles of chloride was accounted for at the end of the test.

Summary

Experiments conducted on cells containing TCE at concentrations above saturation in water indicate that non-aqueous phase TCE does move toward the cathode. The mechanism for this motion is not known. It is not likely electro-osmosis can generate pressure gradients sufficient to push region of DNAPL through the clay matrix. A possible mechanism is that the clay is hydrated with several layers of water molecules and the DNAPL is surrounded by this hydration water. If

there is enough water on the clay, it is plausible that the applied electric field could cause convection within the water layer which in turn drags the interstitial TCE along. While the present work cannot elucidate on the actual mechanism, it does show the TCE in all four experiments was either removed completely or at least transported toward the cathode. In Experiments 7 and 8 it is possible that dissolution and convection of saturated TCE/water was the mechanism of transport. In Experiments 6 and 9 it appears that TCE was transported by direct convection of DNAPL at a rate of approximately 1/6 to 1/10 of the electro-osmotic flow. If we extend these results to field conditions in which non-aqueous phase TCE exists, it appears that approximately 10 pore volumes of electro-osmosis is required to move one pore volume of DNAPL. If we allow two additional pore volumes of purging after the DNAPL is removed, then an upper limit of 12 pore volumes is required in soils containing non-aqueous phase TCE.

K. Modeling Phase IIa Pilot Test

Introduction

The thermal model developed in Phase I was used to predict the thermal behavior and to suggest operating conditions for phases IIa and IIb. A brief description of the model formulation is provided below. The model was described in more detail in the Phase I Topical Report for Tasks 2-4.

Model

The coupled equations describing the electric and temperature fields are

Charge conservation: $\nabla \cdot \sigma(T) \nabla \phi = 0$ **Eq.11**

Combined electroosmotic and hydraulic flow through porous media: $u = -\frac{k_e(T)}{n} \nabla \phi - \frac{k_h(T)}{n} \nabla p$ **Eq.12**

Energy conservation: $\frac{\partial T}{\partial t} = \frac{k}{\rho c} \nabla^2 T - nu \frac{\rho_w c_w}{\rho c} \cdot \nabla T + \frac{\sigma(T)}{\rho c} \|\nabla \phi\|^2$ **Eq. 13**

where ϕ is the electric potential, σ the electrical conductivity, T the soil temperature, ρ the soil density, c the specific heat of the soil, ρ_w the pore water density, c_w the pore water specific heat, n the soil porosity, k the thermal conductivity, and u the pore fluid velocity. Eq. 11 makes several simplifying assumptions regarding charge transport in the soil. First, there are no capacitive effects, which should be the case with a DC electric field. Second, charge is transferred predominantly by ionic migration, so that convection in the charged double layer at the soil particle/pore liquid interface and current carried by diffusion of ions is negligible. And third, the electrical conductivity, to first order, is a function of temperature only.

Because both fluid viscosity and electrical conductivity are very sensitive to temperature, their temperature dependence has been incorporated in this model. The viscosity dependence is reflected by the electro-osmotic permeability, k_e, which varies inversely with viscosity, according to the Helmholtz-Smoluchowski equation. That is, the effects of temperature on the zeta potential, dielectric constant, and solubility of species are ignored. The following expression was used to relate the temperature dependence of the electro-osmotic permeability to the fluid (water) viscosity:

$$\log_{10}\left(\frac{k_e(T)}{k_e(20^\circ\,\mathrm{C})}\right) = -\log\left(\frac{\mu(T)}{\mu(20^\circ\,\mathrm{C})}\right) = \frac{1.3273(T - 20^\circ\,\mathrm{C}) + 0.001053(T - 20^\circ\,\mathrm{C})^2}{(T - 20^\circ\,\mathrm{C}) + 125} \quad \textbf{Eq. 14}$$

Laboratory experiments determined that the temperature dependence of soil electrical conductivity can also be expressed as a function of fluid viscosity. This was expressed as

$$\sigma(T) = \sigma(20^\circ\,C)\,\frac{\mu(20^\circ\,C)}{\mu(T)} \qquad \textbf{Eq. 15}$$

Two-dimensional geometries are used in this analysis. The two-dimensional representation ignores the width of the site and, in effect, assumes the electrodes are infinitely long. Corrections are made to the calculated current and power in order to approximate the third dimension. For Phase IIa, the treated area has two 30 foot wide electrode rows, spaced 20 feet apart. The electrodes extend 45 feet deep. In phase IIb, there are four rows of 60 foot wide electrodes spaced 35 feet apart. The electrodes in IIb also are 45 feet deep. The thermal boundary conditions are constant temperature of 15°C at the soil surface and at the domain bottom where groundwater flow is assumed to maintain a constant temperature. The electrical boundary conditions are ϕ (cathode)=0 and for constant applied voltage ϕ (anode)=ϕ_0. For constant current simulations, the anode boundary condition is $\int_{\text{anode edge}} i dA = I_0$. The parameters used in the example computer simulation are given in Table K-1. Parameters related to soil properties, with the exception of thermal conductivity, were determined from laboratory tests conducted by Monsanto. The soil thermal conductivity was the only property chosen to yield good agreement between the model and pilot test data. The good agreement between model prediction and measurements made in the Phase I pilot test serves to validate the model and parameter values.

Table K-1. Model Parameters

Parameter	Value
Porosity, n	0.4
Thermal conductivity, k	1 W m^{-1} K^{-1}
Electrical conductivity, σ_0(20°C)	0.024 S m^{-1}
Pore fluid viscosity, μ(20°C)	0.001 kg m^{-1} s^{-1}
Soil density, ρ	1970 kg m^{-3}
Soil heat capacity, c	1870 J kg^{-1} K^{-1}
Water density, ρ_w	1000 kg m^{-3}
Water heat capacity, c_w	4180 J kg^{-1} K^{-1}
Electro-osmotic permeability, k_e(20°C)	$1 \cdot 10^{-9}$ m^2 V^{-1} s^{-1}

Results

Phase IIa

The results of the model predictions for Phase IIa are summarized Figures K-1 - 37. In Figure K-1, the maximum temperature occurring in the core of the treated soil is plotted vs. time. A constant current of 192 A was applied to the electrodes. This current was chosen to prevent overheating of the soil while also achieving approximately 1 pore volume of electro-osmotic purging in 90 days when the treatment zone spacing is 2 feet. The pore volumes of electro-osmosis passing through the 2-foot spaced treatment zones is plotted in Figure K-2. The constant flow rate, as indicated by the uniform slope of pore volumes vs. time, represents the cancellation of two effects. As the temperature rises from Joule heating, the fluid viscosity decreases and therefore the electro-osmotic permeability increases. However, with increasing temperature, the electrical conductivity increases, causing the electric field to decrease, given the constant current

boundary condition. The applied voltage, shown in Figure K-3, decreases from an initial value 207 V to 121 V after 100 days. The power, which is the product of the current and applied voltage, starts out at 39.8 kW and drops to 23.5 kW after 100 days.

It is likely that in a full-scale application it may be advantageous to operate at current densities that cannot be sustained because of overheating of the soil. These simulations show that 192 A will lead to temperatures of approximately 85°C after 200 days. The effect of reducing the current by 33% at 100 days is also shown in Figures J-10 and K-1 and K-2. The maximum temperature stays fairly constant with the lower current density, rising only approximately 5°C in 100 days. Since the flow rate is proportional to the electric field, which is in turn proportional to the applied current, the time required for the second pore volume increases by 33%. The applied voltage is also nearly constant after the current reduction because the voltage is a direct function of the temperature field. The power after the current reduction is significantly reduced to approximately 10 kW.

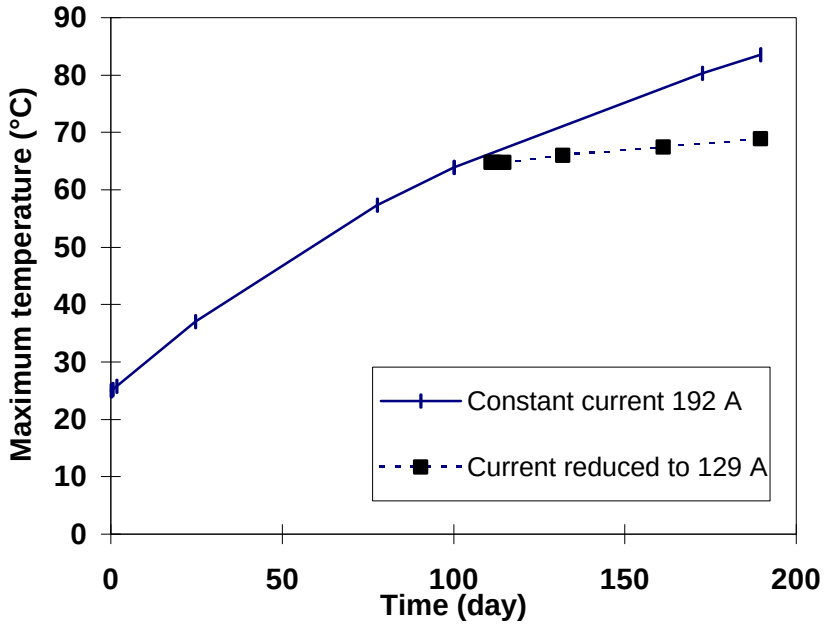

Figure K-1. Temperature predicted in Phase IIa operating at 192 and 129 A.

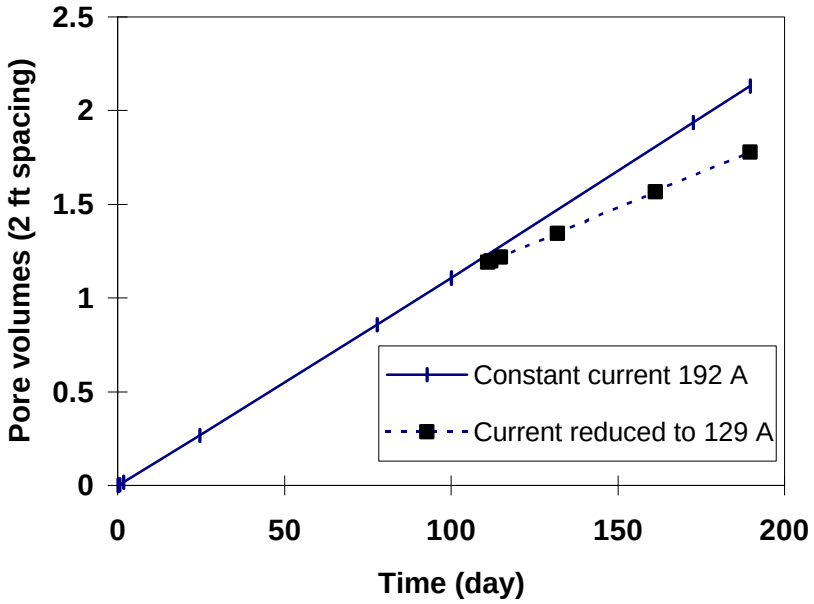

Figure K-2. Pore volumes removed in Phase IIa at 192 and 129 A.

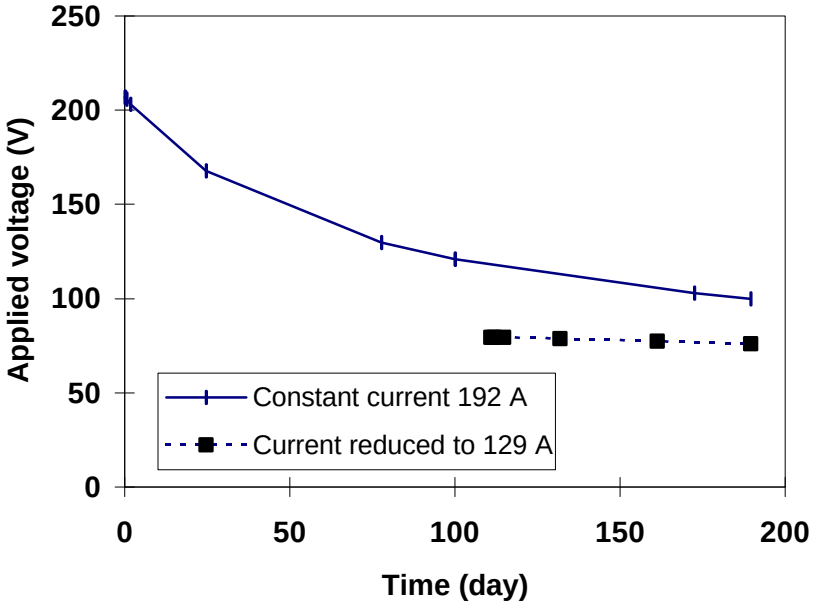

Figure K-3. Voltage response in Phase IIa when operated at a constant current of 192 and 129 A.

The temperature distribution for the Phase IIa simulation of 192 A for 100 days is shown in Figure K-4. The parameters in the figure are nondimensionalized. The maximum temperature is 64°C, and each contour line represents a 5.7°C difference. The thermal boundary conditions are 25 °C at the surface and 7.2°C at 90 ft. There is negligible heating in the top 4 ft of soil. It is assumed that this is because the top 4 ft is a zone of unsaturated sand and gravel.

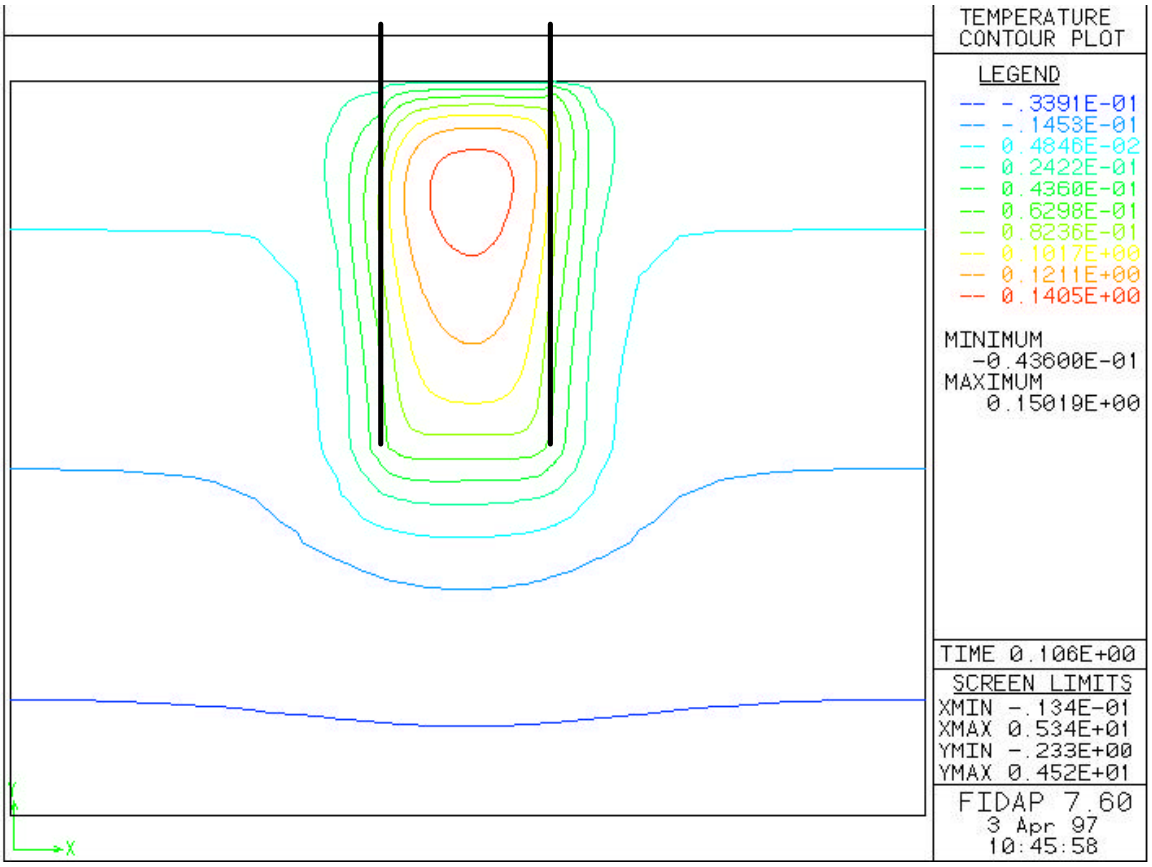

Figure K-4. Temperature distribution after 100 days.
(The parameters in the figure are nondimensionalized. Each contour line represents a 5.7°C difference and the maximum temperature is 64°C. The positions of the electrodes are indicated by the bold vertical lines; the anode is on the left. The length scale is normalized by the electrode spacing of 21 ft.)

A comparison of the model predictions with the field test measurements is shown in Figure K-5. The comparison is made at the centerline of the site, and good agreement is apparent at the depths of 5, 25, and 50 ft. It should be pointed out that the current applied in the early stages of the field tests ranged from 122 A to 162 A for the first 50 days. However, during this time there was a significant AC component to the applied field because of a mismatch in generator and rectifier voltages. The AC component heats the soil just as the DC component does, so modeling the first 50 days with 192 A is not unreasonable. The agreement between model and experiment after 50 days, when the field and model conditions were the same, validates the assumptions made in the model. The agreement between the model and experiment is also very good when the horizontal temperature distributions are compared. Figure K-6 shows a plot of the temperature at 25 ft after 100 days of operation.

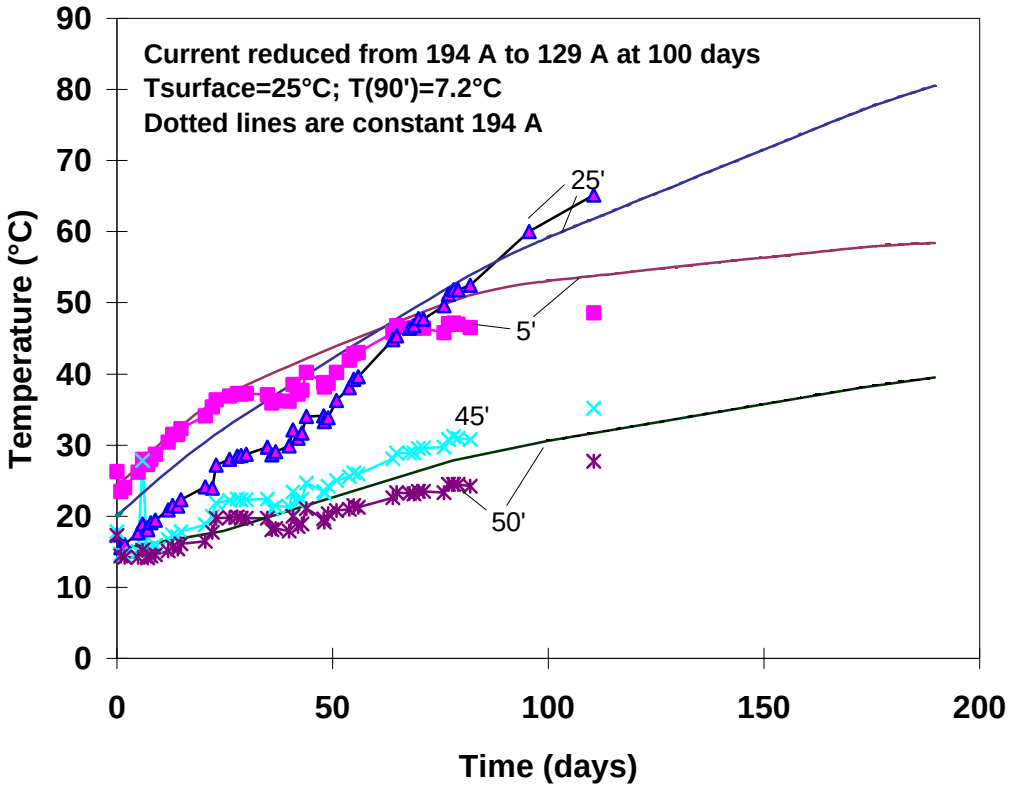

Figure K-5. Comparison of model prediction to field test data at 5, 25, 45, and 50 ft depths.

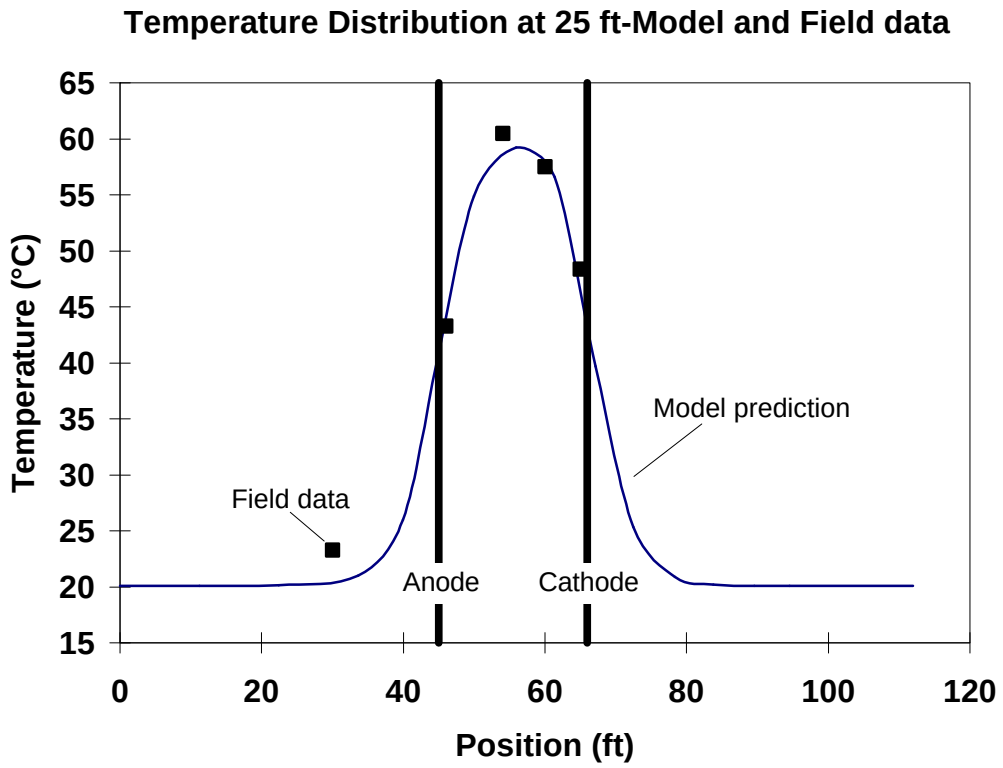

Figure K-6. Comparison of measured and predicted temperature profile in Phase IIa at 25 ft depth after 100 days.

Phase IIb

The results of the model simulation for Phase IIb are summarized in Figures K-6 through K-8. The simulation shows an initial current of 1,045 A for 137 days, followed by a current of 700 A for the next 400 days. The applied currents were chosen to achieve 2 pore volumes of purging through 7-foot spaced treatment zones in approximately 1.5 years. It is apparent in Figure K-7 that the temperature will exceed 100°C after approximately 200 days if the current is maintained at 1,045 A. Reducing the current by 33 % after 137 days allows the system to operate an additional 300 days before boiling occurs in the hot region. The maximum voltage applied between adjacent electrodes is 388 V at the start of the remediation. By 137 days, the voltage is reduced to 171 V as a result of the increase in electrical conductivity due to heating. The voltage is then reduced to 114 V to reduce the current density.

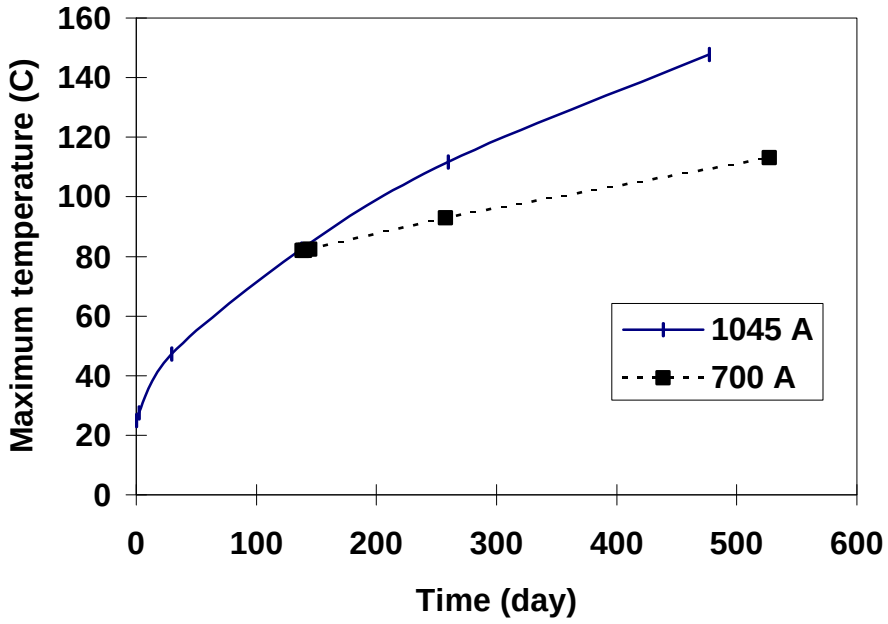

Figure K-7. Maximum temperature vs. time predicted for Phase IIb operating at 1,045 and 700 A.

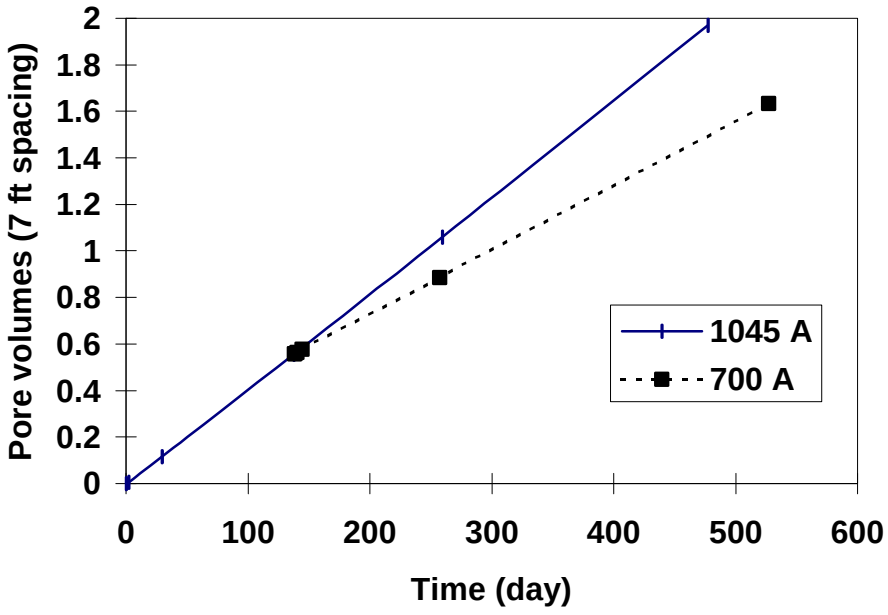

Figure K-8. Pore volumes removed for Phase IIb with treatment zones spaced at 7 ft intervals.

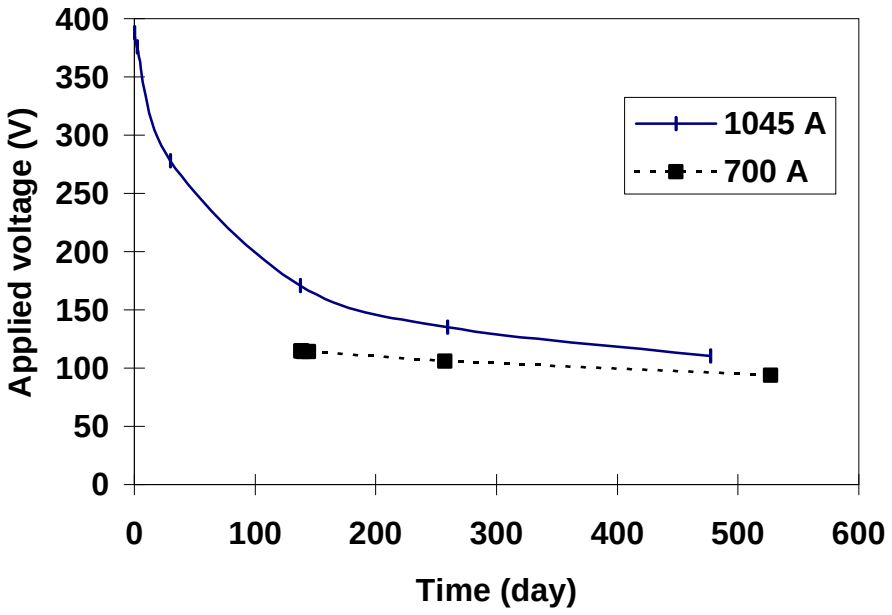

Figure K-9. Voltage response to constant current operation of Phase IIb.

The temperature distribution for the Phase IIb simulation of 1,045 A for 137 days is shown in Figure K-10. The parameters in the figure are nondimensionalized. The maximum temperature is 82°C, and each contour line represents a 7.5°C difference. The thermal boundary conditions are 25°C at the surface and 7.2°C at 90 ft.

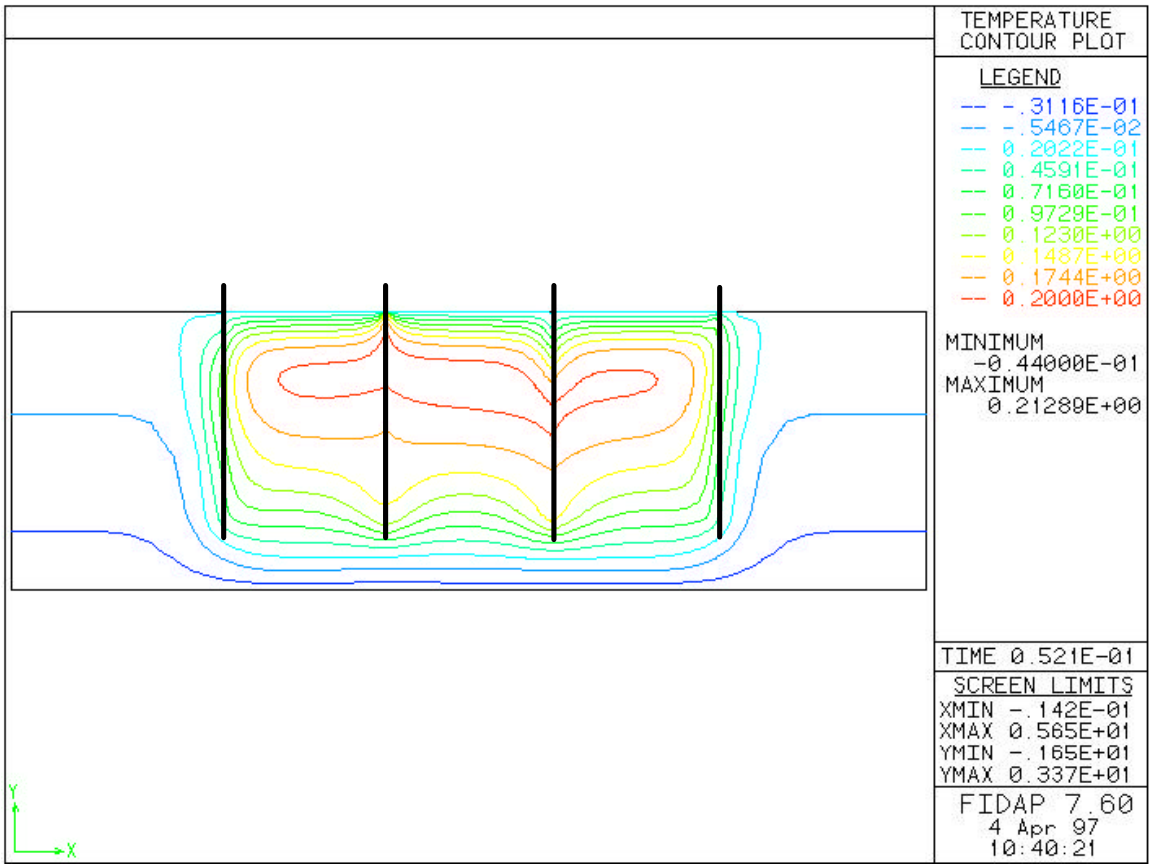

Figure K-10. Temperature field generated in Phase IIb after 137 days. (The parameters in the figure are nondimensionalized. Each contour line represents a 7.5°C difference and the maximum temperature is 82°C. The positions of the electrodes are indicated by the bold vertical lines; the leftmost electrode is an anode and the polarity of adjacent electrodes is opposite. The length scale is normalized by the electrode spacing of 35 ft.)

Streamlines marking the extent of electro-osmotic flow are shown in Figure K-11. The streamlines emanate from treatment zones adjacent to the electrodes and indicate the trajectory of the flow for the initial 137 days of the simulation. The horizontal dashes below the streamlines indicate the 7-ft spacing between treatment zones. As indicated in Figure K-8, approximately 0.6 pore volume have been passed between treatment zones at this point.

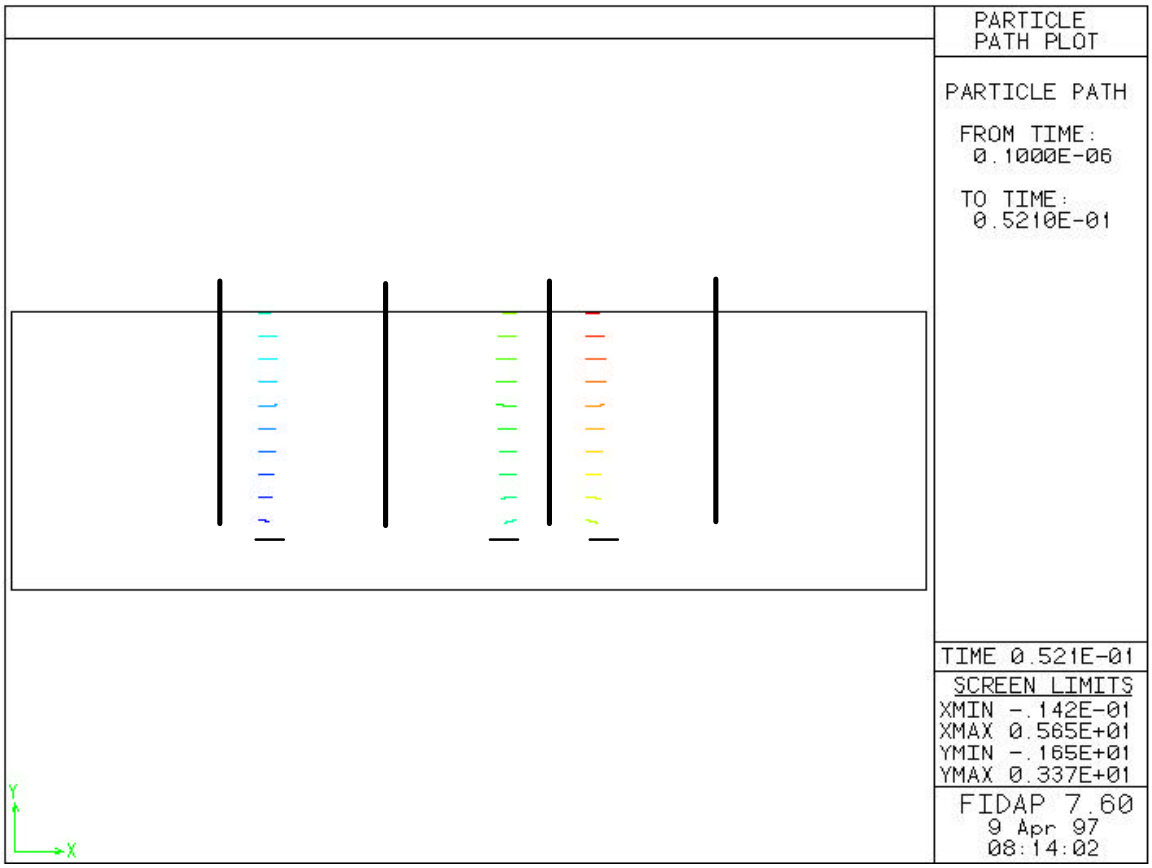

Figure K-11. Streamlines in Phase IIb.

(Streamline paths are calculated 137 days of operation at 1,045 A. The vertical lines represent electrode position, and the horizontal dashes represent treatment zone spacing of 7 ft. Streamlines emanate from treatment zones adjacent to anodes.)

References

Topical Report for Tasks No. 2-4, DOE Contract Number:DE-AR21-94MC31185, 1996

Topical Report for Task No. 9, DOE Contract Number:DE-AR21-94MC31185, 1996

Reardon (ES&T '95, 29**,** 2936-2945)

L. Improvements in Treatment Zone Technology Research

Hydrogen Evolution: Implications to Iron Selection

Permeable reactive barriers have been shown to be a cost-effective alternative to pump-and-treat systems in capturing and degrading contaminants in medium- to high-permeability soils and aquifer. To date, greater than one dozen pilot- or full-scale installations employing granular iron have been installed in the field.

The application of granular, zero-valent iron in low permeability soils, however, poses additional challenges. For example, as iron corrodes in aqueous systems, hydrogen gas is released via the reaction shown in Eq. 16. If the hydrogen production is slow enough, the gas will remain dissolved in the pore water and will be convected away by electro-osmosis. If the hydrogen production is fast and/or the solubility of the gas decreases because of temperature effects, hydrogen bubbles may form and become trapped in the treatment zone. Laboratory experiments conducted at GE in test cells showed that if hydrogen is trapped in the granular iron treatment zone, electro-osmotic flow can be adversely affected. Electrochemical reactions occurring at the anode are predicted to alter the pH and will also affect the reductive dissolution rate of the iron metal. Fortunately, there is no explosion hazard for hydrogen, as the hydrogen concentrations predicted in iron/clay treatment zones are several orders of magnitude below the explosion limit for hydrogen.

$$Fe^0 + 2H_2O \rightarrow Fe^{2+} + H_2 + 2OH^- \qquad \text{Eq. 16}$$

Concurrent with studies to more closely evaluate the effect of trapped hydrogen on electro-osmotic flow, a study was undertaken to evaluate hydrogen evolution rates of commercial, low-cost granular iron in aqueous and aqueous-clay suspensions. A slower corrosion rate in a particular iron-water system would also mean a slower degradation rate for the chlorinated solvent, as the latter reaction is also corrosion-mediated (Eq. 17) However, if hydrogen evolution in the treatment zone seriously compromised electro-osmotic flow, the selection of a more corrosion-resistant iron material could be necessary. An average hydrogen generation rate of approximately 0.5 mmol/kg iron/day was anticipated, based on previous reports (Reardon, 1995).

$$Fe^0 + RCl + H_2O \rightarrow Fe^{2+} + RH + Cl^- + OH^- \qquad \text{Eq. 17}$$

A selection of different mesh sizes of granular iron supplied by Peerless Metal Powders and Abrasive and Connelly-GPM, and micropowder iron from ISP (grade S-3700) were reacted in batch mode with deionized water over a period of 4 weeks. Hydrogen evolution was monitored using a GC-MS technique. Generalized results are summarized in Table L-1. As expected, the higher surface area iron afforded faster rates of hydrogen evolution. The addition of kaolin clay to the granular iron, while buffering the aqueous phase to some degree, did not appreciably affect the hydrogen evolution rate.

Table L-1. Comparison of hydrogen evolution rates measured in batch reactors. Reactors contained 25 g iron/75 mL deionized water or 25 g iron/50 g kaolin clay/25 mL deionized water, as specified.

System	Iron source	Iron surface area, m^2/g	Hydrogen evolution
Iron/water	Peerless -50 mesh to dust	2.16	medium
Iron/water	Peerless -20 mesh to dust	1.54	medium
Iron/water	Peerless -8+50 mesh to	0.98	low
Iron/water	Connelly GPM, -6+16 mesh	1.75	medium
Iron/water	ISP micropowder iron	1.0	high
Iron/kaolin/ Water	Peerless -20 mesh to dust	1.54	medium

Reductive Dechlorination of Solvents by Iron(II) Mineral

Fe(II) complexed to organic ligands and Fe(II) bound to O^{2-} in solid phases or as hydroxo complexes are also stronger reductants relative to Fe(II) itself. Fe(II) complexes and Fe(II) minerals, therefore, may also participate in the reduction of alkyl chlorides, as in Eqs. 18 and 19.

$$2Fe^{2+}(\text{complex}) + RCl + H^+ \rightarrow 2Fe^{3+}(\text{complex}) + RH + Cl^- \qquad \text{Eq. 18}$$

$$2Fe^{2+}(\text{solid phase}) + RCl + H^+ \rightarrow 2Fe^{3+}(\text{solid phase}) + RH + Cl^- \qquad \text{Eq. 16}$$

Recently, we have proposed that the reduction of chlorinated hydrocarbons by iron metal occurs by a reaction of surface-bound Fe(II) at the iron metal-water interface (Sivavec and Horney, 1995). The surface-bound Fe(II) species at the passive oxide-water interface most likely serves as mediator for the transfer of electrons from Fe^0 to adsorbed chlorinated hydrocarbon. The mediation of redox reactions by Fe(II)/Fe(III) in natural environments is also attributed to the role of this accelerated pathway for electron transfer (Figure F-1). Such redox reactions are responsible for reduction of metal ions and organic compounds in the environment and may be classified as natural attenuation processes.

Recent studies have shown, for example, that surface-bound, reduced-iron species play the important role of electron transfer mediator in reductions promoted by iron-reducing bacteria (Heijman *et al*. 1995) and iron hydroxide surfaces to which Fe(II) has been adsorbed (Klausen *et al.* 1995).

The high specific surface areas of iron-bearing minerals [Fe(II,III)] hydroxides, iron sulfides, Fe(II)-silicates) and the reduced redox potential of a surface-bound Fe(II) species relative to aqueous Fe(II) often facilitate transformations of reducible organic substances in natural systems. Surface-bound Fe(II) species may serve as mediators in the transfer of electrons from a bulk reductant to reducible chlorinated compounds (Figure L-1).

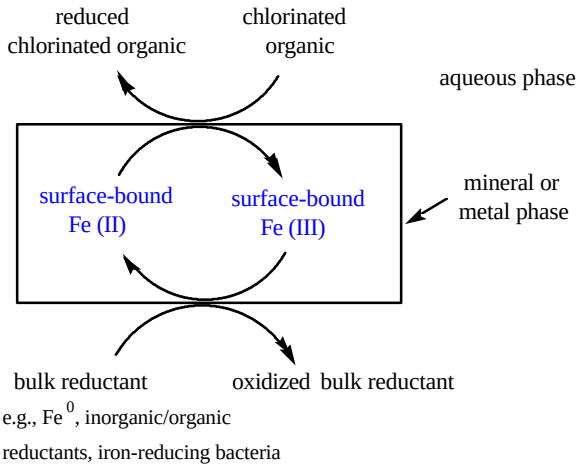

Figure L-1. General reaction scheme for chlorinated solvent reduction at Fe(II) sites.

Recently, it has been postulated that the reduction of chlorinated hydrocarbons by zero-valent iron may occur by a reaction of surface-bound Fe(II) at the iron metal-water interface (Sivavec and Horney, 1995; Klausen *et al.* 1995. Surface characterization of granular iron and kinetic studies further suggest that grain-scale diffusion of the chlorocarbon through the oxide film to the reactive Fe(II) site may explain mass transport effects commonly observed in batch and column systems (Burris *et al.* 1995).

Fast reduction rates for chlorinated hydrocarbons observed in the zero-valent iron system may be attributed to the facile regeneration of reducing surface Fe(II) species due to the proximity of the bulk reductant (Fe^0) to the electron carrier, surface-bound Fe(II). A reduction mechanism mediated by Fe(II)/Fe(III) may be considered a refinement of a direct electron-transfer mechanism. It takes into account that iron metal surfaces are protected by a passive film of iron oxide and that the interface between the aqueous alkyl halide and the iron metal surface is this passive oxide. Fe^0 remains the bulk reductant and Fe(II)/Fe(III) serves as the electron transfer mediator.

Our interest in understanding the interaction of chlorinated solvents within iron oxide films at iron metal surfaces has led us to investigate the redox properties of a number of Fe(II) and Fe(II,III) minerals including magnetite (Fe_3O_4) and troilite (FeS). The redox properties of magnetite, a mixed oxide, are of particular interest in that the passive film at iron metal surfaces consists of an inner layer of magnetite (and an outer layer of maghemite, γ-Fe_2O_3). In addition, reductive transformations mediated by magnetite surfaces may contribute to natural attenuation processes controlling the fate of pollutants in soils, sediments, and aquifer materials.

Reductive dechlorination of chlorinated ethenes such as TCE, DCE, and VC promoted by magnetite and troilite was previously studied in batch and column systems. First-order rate constants for TCE, normalized to mineral surface areas, are given in Table L-2. When normalized to surface area, specific rate constants describing TCE degradation (k_{SA}, $Lh^{-1}m^{-2}$) in zero-valent iron, troilite, and magnetite studies are remarkably similar, differing at most by one order of magnitude. First-order rate constants for individual halocarbons determined for various sources of zero-valent iron alone have been shown to vary by one order of magnitude (Johnson *et al.* 1996). That the TCE dechlorination rate for magnetite differs by as little as a factor of 3 from that determined for granular iron argues that magnetite sites at

the zero-valent iron surface may be mediating electron-transfer processes in granular iron systems.

Table L-2. Comparison of surface area-normalized first-order TCE dechlorination rate constants, kSA, measured in granular iron, iron sulfide, and magnetite systems.

System	water	redox-active media	[surface area] m2 / L	kobsd, h-1	half-life, h	kSA, Lh-1m-2
Column	site gw	granular iron	4210	0.337	2.06	8.0 x 10-5
Column	site gw	granular iron	4760	0.271	2.55	5.7 x 10-5
Column	site gw	troilite, FeS	1050	0.792	0.9	7.5 x 10-4
Batch	deionized	magnetite, Fe3O4	81	0.00152	454	1.9 x 10-5

The effect of FeS surface area concentration (m^2/L) was further studied by varying the FeS mass in batch experiments. A pseudo-first-order dependence of reduction rate on chloroethene concentration was determined in the presence of 0.125 to 25 m^2/L FeS. A linear relationship between the FeS surface area concentration (m^2/L) and pseudo-first-order rate constant for TCE loss, k_{obsd} (h^{-1}) is shown below, relative to the same relationship determined for granular iron.

$$k_{obsd} = 8.680 \times 10^{-4} \text{ [FeS surface area, } m^2/L] + 0.000716 \qquad (r^2=0.998)$$

$$k_{obsd} = 1.926 \times 10^{-4} \text{ [granular iron surface area, } m^2/L] + 0.000193 \quad (r^2=0.964)$$

Product distributions and intermediates were very similar in the FeS, magnetite, and Fe^0 systems, further suggesting that common reduction pathways are followed. Chlorinated ethenes were reduced via two degradation pathways: (a) reductive β-elimination and (b) sequential hydrogenolysis. The two pathways result in different intermediates, but may lead to similar hydrocarbon products. Reductive β-elimination of TCE leads to chloroacetylene, a very short-lived intermediate that is further reduced to acetylene (Roberts *et al.* 1996). A minor pathway also hydrolyzes chloroacetylene to acetate (typically <5% of products). Sequential hydrogenolysis reduces TCE stepwise to DCE, VC, and ethene. In the zero-valent iron system, further reduction to ethane is often observed.

The major hydrocarbon product in the FeS systems was acetylene. In Fe^0 batch and column systems, acetylene was further reduced to ethene and ethane. Significantly smaller concentrations of C3-C6 hydrocarbon products were observed, consistent with the coupling of intermediate carbon-centered radicals at the iron metal and FeS surface. Experiments employing $^{13}C_2$-labeled TCE verified that all C2-C6 hydrocarbon products originated from TCE and that CS_2 and CO_2 were not produced from TCE. XPS analysis of the native FeS surface indicated only oxidized forms of sulfur and no sulfide. This and other data suggests a mechanism of chloroethene reduction promoted by surface-bound Fe(II) or possibly protonated iron sulfide surface groups and not by surface-bound sulfur species as seen in the pyrite/carbon tetrachloride system (Kriegman-King and Reinhard 1994).

Screening Study: Mined Minerals as the Source of Iron Material

Several research groups have proposed that ferrous bound to iron mineral surfaces can act as a reductant, mediating the electron transfer to nitroaromatics (Klausen *et al.*, 1995;

Heijman *et al*., 1995) or chlorinated hydrocarbons (Sivavec and Horney, 1995). Thus, manipulation of natural iron minerals to increase the amount of surface-bound ferrous ion could produce reactive material for remediating chlorinated hydrocarbons such as TCE. In a *Lasagna*™ application, natural iron oxides such as magnetite, goethite, or hematite (or mixtures thereof) would serve as treatment zones. These potentially reactive materials could be filled into treatment zones, or more economically, native iron oxides would be present at high enough concentration in the highly impermeable soil such that they would need only to be activated by an appropriate reducing agent or soluble ferrous ion.

Previously, laboratory-prepared magnetite has been shown to dechlorinate TCE, DCE, VC and other chlorinated solvents at rates approaching that of zero-valent iron when surface areas are normalized (Sivavec and Horney, 1997). Other primary minerals in soil contain iron as well; biotite, hornblende, and olivine are some examples of common iron silicates (Tan, 1994). The purpose of this task was to determine whether readily available natural iron minerals could be manipulated to become reactive and dechlorinate TCE at a cost less than that of granular iron from current suppliers.

Therefore, a process was sought by which native iron minerals and/or iron-bearing clays in an aquifer would be reduced, thereby generating redox-active zones. If successful, this approach should greatly reduce the costs associated with the emplacement of zero-valent iron treatment zones in *Lasagna*™ applications. Reactive zones as such have been produced by the addition of sodium dithionite, a strong inorganic reductant, in buffered aqueous solution to a chromium-contaminated aquifer at the Hanford site in Richland, Washington. Considerable laboratory work has also focused on reduction of chlorinated solvents by dithionite-reduced clays and sediments (Amonette *et al*., 1994, Amonette *et al*., 1995).

A screening study was undertaken to identify potential natural iron minerals that might be effective in an electro-osmotic field treatment zone as well as identify specific amendments that could be added to an aquifer, creating a reactive zone in which TCE would be destroyed *in situ*. This approach has implications for use particularly in deep, contaminated aquifers. Freshly-mined goethite, magnetite, hematite, biotite, hornblende, and olivine were purchased from Ward's Natural Science Establishment, ground in a porcelain pebble mill, and wet screened through a 20 micron screen by Lakefield Research Limited. These minerals were stored in a nitrogen tent until used in our screening batch study. We purchased freshly mined minerals so that any passivation layer on the minerals would be natural and not a result of the storage of the solids in air. The minerals were then treated with a variety of reductants or ferrous compounds in a batch experiment to study the effect on the dechlorination of TCE. Table L-3, following, characterizes the iron minerals that were used.

Table L-3. Iron Minerals Used in Screening Study.

Iron Mineral	Surface Area (m^2/g)*	Percent Iron	Extractable Ferrous Iron (mg/kg)	Percent Extractable Ferrous Iron of Total Iron
Goethite	63.64	29	9.44	0.003
Magnetite	2.96	79	59.3	0.008
Hematite	3.06	55	34	0.006
Biotite	19.57	9.0	190	0.211
Hornblende	9.92	3	18.5	0.062
Olivine	1.01	2	25.8	0.129

**Surface area measured by BET gas adsorption.*

Sodium salts of oxalate, ascorbate, or citrate were tested as reductants as well as sodium hydrosulfite (dithionite) and sodium bisulfite. Ferrous sulfate was tested as a supplemental source of ferrous ions, while disodium EDTA was used as a treatment to solubilize the iron in the minerals. Vitamin B12 was also included as a possible dechlorination catalyst. The variables of this test are summarized below.

Iron minerals:

Goethite	Biotite
Magnetite	Hornblende
Hematite	Olivine

Reductants/Catalysts:

Sodium oxalate	Sodium hydrosulfite	EDTA
Sodium ascorbate	Sodium Bisulfite	Vitamin B12
Sodium citrate	Ferrous sulfate	

The screening tests were run in 50-ml serum bottles. Approximately 20 ppm TCE was added to sodium bicarbonate buffer, which was then added to the serum bottles containing six grams of iron mineral and/or 10 mM reductants/catalysts. In addition, two controls were set up: iron minerals without a reductant or catalyst, and some of the reductants/catalysts without iron minerals. A zero and four-week time points were taken (after rotating on a jar mill) and the aqueous phases were sampled and analyzed by GC/FID equipped with a purge-and-trap autosampler. Samples were analyzed for chlorinated as well as nonchlorinated hydrocarbon products.

In order to determine whether a specific amount of dechlorination was to be considered a positive result (thus requiring a more focused effort), a speadsheet was developed to relate the extent of dechlorination in batch experiments with a desired TCE half-life under field conditions. Variables in the spreadsheet included percent iron in soil, ground water velocity, and dimensions of a given treatment zone. By choosing an acceptable half-life given typical field conditions, it was easy to determine how much TCE reduction or products produced would be required for us to consider a certain treatment "successful" in terms of enhancing

TCE dechlorination. For these experiments, it was clear that TCE reduction could be very small even in "successful" treatments. Therefore, it was necessary to measure dechlorination products (cis-DCE, VC, ethene, ethane, acetylene). The identification of dechlorination products (concomitant with reduction in TCE) was important since we were not able to verify dechlorination by analyzing for chloride ions in the presence of the iron minerals.

Results and Discussion

The results of this screening showed that activity was dependent upon the reductant/catalyst as well as the type of iron mineral, although the reductant/catalyst appeared to be more important. None of the iron minerals effected TCE dechlorination without amendment with a chemical reductant. Although the concentration of TCE was reduced in all of these bottles, no dechlorination products were identified, and the amount of TCE lost in these controls was the same regardless of the iron mineral used. It is assumed that the decrease in TCE was due to physical losses into the septum or adsorption onto the minerals. Also, no dechlorination occurred in bottles amended with oxalate or citrate. Some of the amendments such as ascorbate, EDTA, vitamin B12, and sodium bisulfite resulted in dechlorination. These compounds were not effective in all of the minerals tested; only a few isolated cases resulted in a significant reduction in TCE. In most of these batch experiments, however, dechlorination products were not identified, and so no further conclusions were reached approximately these treatments. The most important finding from this screening study was not so much identifying a natural iron mineral that effected dechlorination of TCE under several treatment conditions, but rather that sodium hydrosulfite and the ferrous sulfate treatments showed promise in several of the iron minerals tested.

In our screening, TCE was reduced to cis-DCE, VC, ethene, and/or ethane in bottles containing magnetite, hornblende, olivine, or no mineral and dithionite. The TCE decreased by 25% in the bottle with no mineral or hornblende, 41% in the bottle with olivine, and as much as 83% in the bottle containing hornblende. Dithionite is a very strong inorganic reductant and has been shown to reduce redox-sensitive compounds, such as iron-containing compounds, in soil (Amonette et al., 1994). Depending on the structure of the iron minerals present, the ferrous iron may remain associated on the surface of the iron minerals, which could lead to an increase in the number of reactive sites on the surface of that mineral. It is hypothesized that, in the experiment, dithionite did indeed reduce the iron minerals, resulting in an increase in Fe (II) and the dechlorination of TCE. Based on that report, and the findings of this screening batch study, there is a need to study further the potential for using dithionite in a remediation scheme for destroying TCE, particularly in deep aquifers.

Based on the hypothesis that the surface-bound Fe (II) species at the passive oxide-water interface serves as the mediator for the transfer of electrons from iron minerals (Sivavec and Horney, 1995), some of the minerals were amended with ferrous sulfate to determine whether supplemental ferrous iron would enhance the dechlorination activity. In some of the iron mineral slurries, the TCE decreased by 10% and as much as 40% in the olivine slurry. The dechlorination products identified were cis-DCE, VC, and/or ethene. Several times, however, no known dechlorination products were identified. Although these decreases in TCE seem small, they are indeed significant in terms of our criteria for a successful treatment, based on the desired TCE half-life. Thus, the addition of ferrous iron

to the iron minerals did seem to increase the destruction of TCE, and one might envision a remediation scheme in which the available ferrous iron is supplemented in the reactive zone.

Summary of Iron Mineral Screening Study

Natural, freshly-mined iron minerals (both oxides and silicates) were examined for their ability to effect reductive dechlorination of aqueous TCE. None of the minerals reduced TCE without some sort of amendment. And none of the amendments (reductants or catalysts) induced dechlorination in all of the iron minerals tested. Sodium hydrosulfite and ferrous sulfate were the most promising compounds in terms of inducing dechlorination in several of the iron mineral slurries. Ultimately, use of these amendments could find application in electro-osmotic remediation applications where chlorinated solvents and/or metal ions need to be reduced. This approach for the generation of reactive treatment zones would be useful at sites in which deep aquifer contamination exists and other treatment zone emplacement techniques are not technically feasible or cost effective. Further research and development would be required to determine the extent to which chlorinated solvents at a specific remediation site be reduced by hydrosulfite and other reducing agents.

Effect of High TCE Concentrations on Dechlorination Rate and Reaction Products

As phase IIa field results were obtained, it became clear that substantially higher TCE concentrations were present in the test site relative to those indicated by the pre-test soil samples. Consequently, the designed operation time of 6 months was no longer adequate for cleanup of TCE in the field test site. Although it is difficult to predict how long a period will be required to reduce TCE concentrations to targeted levels due to the uncertainty in DNAPL volume at the site, it was important to determine if the rate of TCE destruction in the iron zones at high TCE concentrations would be different from that measured and designed for at low TCE concentrations. The electrokinetic movement of DNAPL into the iron treatment zones could also influence predicted TCE destruction rates and product distributions. Consequently, a series of batch kinetic studies was undertaken to address these issues. Two determinations of batch kinetics were determined using Peerless -8+50 mesh iron filings at iron surface area concentrations of approximately 100 m^2/L. The rate profiles are given in the following Figures L-2 and L-3 and are compared to rate measurements determined for similar iron surface concentrations at low initial TCE concentrations (<20 mg/L $[TCE]_o$) (Table L-4). As is seen in all batch experiments, the rate order is first-order with respect to TCE, even at high TCE concentrations. Initial TCE concentrations were 1,000 mg/L. Preliminary evaluations of TCE concentrations above its water solubility (1,100 mg/L at 25°C) gave inconsistent results due to the difficulty in sampling a heterogeneous DNAPL/water/iron system. The evolution of products of TCE degradation (chloride and ethene/ethane) was also found to be not significantly different when 1,000 mg/L or 2,500 mg/L initial TCE was used, indicating that only dissolved-phase TCE reacts at the iron surface (Figures L-2 - L-8) .

Table L-4. Comparison of First-Order TCE Reduction Rates Measured in Batch and Column Systems

k_{SA} represents surface-area-normalized first-order rate constant

all rates determined at very low TCE concentrations (< 5 mg/L), except where noted

System	Water	Iron	m2 / L	kSA Lh-1m-2
Batch	DI	Peerless -50 mesh to dust	180	1.9 x 10-4
Batch	DI	Peerless -20 mesh to dust	126	1.7 x 10-4
Batch	DI	Peerless -8 + 50 mesh	variable	1.3 x 10-4
Batch	DI	Peerless -4 + 18 mesh	289	1.0 x 10-4
Batch	DI	Peerless -8+50 mesh at 1000 mg/L [TCE]o	99	4.8 x 10-5
Batch	DI	Peerless -8+50 mesh at 1000 mg/L [TCE]o	100	6.9 x 10-5
Batch	site gw #1	Peerless -8 + 50 mesh	variable	2.5 x 10-4
Column	site gw #1	Peerless -8 + 50 mesh	3810	1.2 x 10-4
Column	site gw #1	Guar Gum and Peerless -8 + 50 mesh	4853	1.9 x 10-4
Column	site gw #2	Peerless -8 + 50 mesh	4210	8.0 x 10-5
Column	site gw #2	Peerless -8 + 50 mesh	4760	5.7 x 10-5

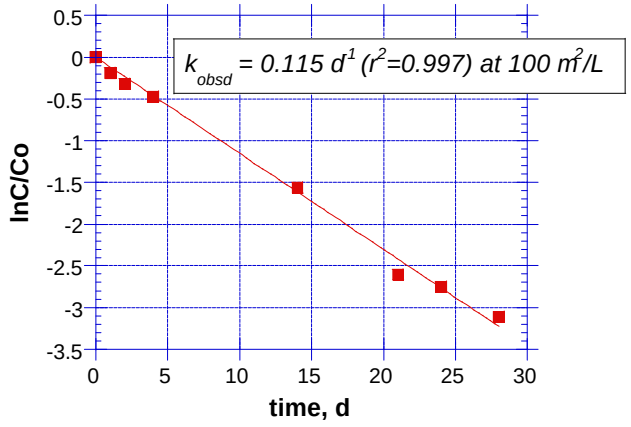

Figure L-2. TCE Degradation Kinetics.

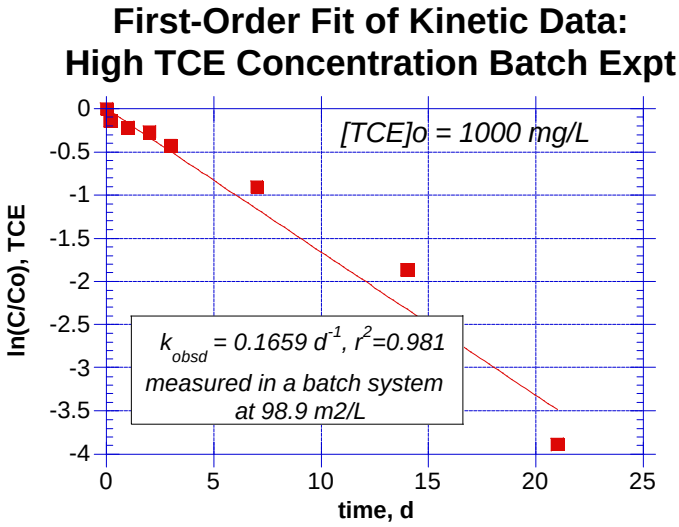

TCE half-life measured in a batch system at low iron surface concentration: 99 h

extrapolation to 4500 m2/L iron surface area predicts a TCE half-life of 2.2 h in a 100% iron zone

Figure L-3. TCE degradation at high concentrations.

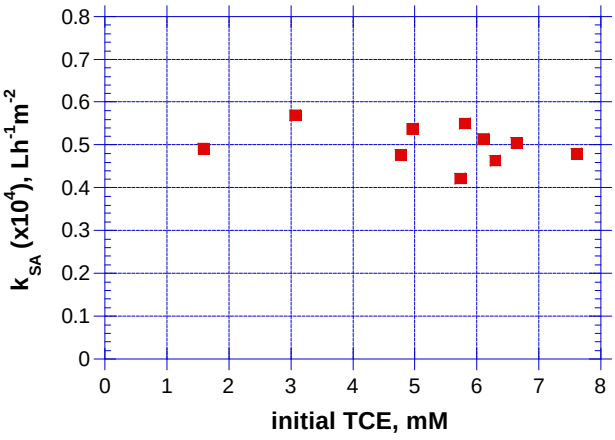

Effect of $[TCE]_o$ on first-order rate constant k_{SA} (surface area normalized) determined in anaerobic batch experiments

Figure L-4. TCE degradation at high concentrations.

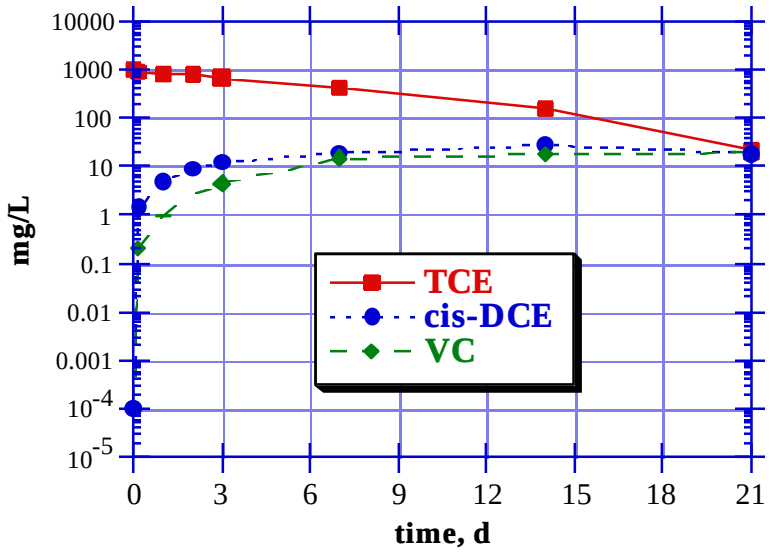

Concentrations of cis-DCE and VC products similar to that measured at low TCE concentration

Figure L-5. Daughter product concentrations during TCE degradation.

Table L-5. Cis-Dichloroethylene and Vinyl Chloride (VC) Formation as a Function of Initial TCE Concentration.

Initial TCE concentration, $[TCE]_o$	% cis-DCE formed, relative to $[TCE]_o$	% VC formed, relative to $[TCE]_o$
1000	2.7	1.9
0.16	2.7 - 3.6	1.6 - 2.1

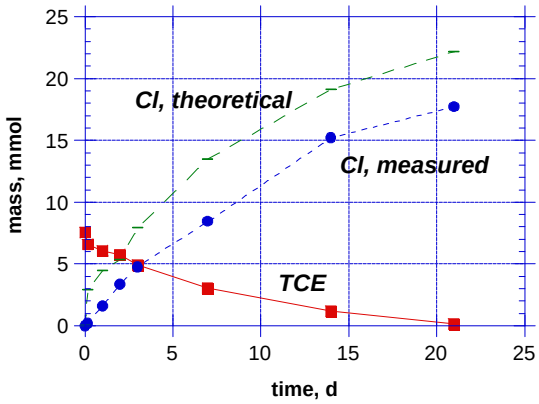

Chloride Mass Balance
Measured at 1000 mg/L [TCE]o

Figure L-6. Chloride mass balance in TCE degradation experiment.

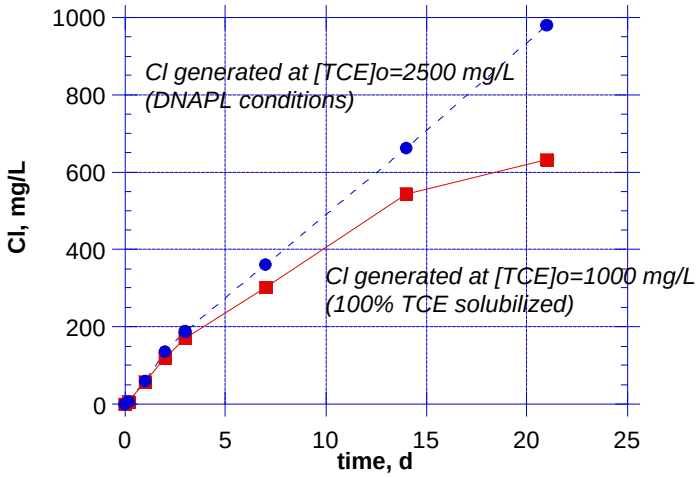

No significant DNAPL destruction
at the iron surface, unless TCE is solubilized

Figure L-7. TCE degradation with DNAPL present.

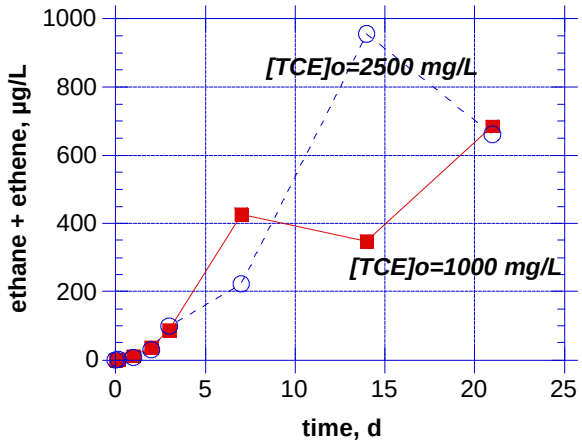

Figure L-8. Generation of ethane and ethene as a function of initial TCE concentration.

References

Amonette, J.E., Szecsody, J.E., Schaer, H.T., Templeton, J.C., Gorby, Y.A., and J.S. Fruchter. 1994. In *In-Situ Remediation: Scientific Basis for Current and Future Technologies*; Gee, G.W.; Wing, R.N., eds.; Battelle Press: Richland, WA; 851-882.

Amonette, J.E., Istok, J.D., Szecsody, J.E., Humphrey, M.D., Williams, M.D., Cole, C.R., Vermeul, V.R., Teel, S.S., Gorby, Y.A., Yabusaki, S.B., and J.S. Fruchter. 1995. *Emerging Technologies in Hazardous Waste Management VII*. ACS Industrial & Engineering Chemistry Division, Sep 17-20, 1995. 588.

Burris, D.R., T.J. Campbell and V.S. Manoranjan. 1995. Sorption of Trichloroethylene and Tetrachloroethylene in a Batch Reactive Metallic Iron-Water System *Environ. Sci. Technol.*, *29*, 2850-2855.

Heijman, C.G., E. Grieder, C. Hollinger, C. and R.P. Schwarzenbach. 1995. Reduction of Nitroaromatic Compounds Coupled to Microbial Iron Reduction in Laboratory Aquifer Columns *Environ. Sci. Technol.*, *29*, 775-783.

Johnson, T.L., M.M. Scherer and P.G. Tratnyek. 1996. Kinetics of Halogenated Organic Compound Degradation by Iron Metal *Environ. Sci. Technol.*, *30*, 2634-2640.

Klausen, J., S.P. Trober, S.B. Haderlein and R.P. Schwarzenbach. 1995. "Reduction of Substituted Nitrobenzenes by Fe(II) in Aqueous Mineral Suspensions" *Environ. Sci. Technol.*, *29*, 2396-2404.

Kriegman-King, M. and M. Reinhard. 1994. Transformation of Carbon Tetrachloride by Pyrite in Aqueous Solution *Environ. Sci. Technol.*, *28*, 692-700.

Roberts, A.L., L.A. Totten, W.A. Arnold, D.R. Burris and T.J. Campbell. 1996. Reductive Elimination of Chlorinated Ethylenes by Zero-Valent Metals *Environ. Sci. Technol.*, *30*, 2654-2659.

Sivavec, T.M. and D.P. Horney. 1997. Reduction of Chlorinated Solvents by Fe(II) Minerals. Prepr. Pap. ACS Natl. Meet., Am. Chem. Soc., Div. Environ. Chem., 37(1).

Sivavec, T.M. and D.P. Horney. 1995. Reductive Dechlorination of Chlorinated Ethenes by Iron Metal and Iron Sulfide Minerals *Emerging Technologies in Hazardous Waste Management VII*, Atlanta, GA; American Chemical Society: Washington, DC, 42-45.

Stumm, W. 1992. *Chemistry of the Solid-Water Interface: Processes at the Mineral-Water and Particle-Water Interface of Natural Systems*. Wiley, New York.

Tan, Kim H. 1994. Environmental Soil Science, Marcel Dekker, Inc.